Nano Research

ISSN 1998-0124 CN 11-5974/O4
https://doi.org/10.1007/s12274-023-5605-2

Research Article

On-surface synthesis and edge states of NBN-doped zigzag graphene nanoribbons

Xiao Chang[1,§], Li Huang[1,§], Yixuan Gao[1,§], Yubin Fu[2,§], Ji Ma[2,3], Huan Yang[1], Junzhi Liu[4], Xiaoshuai Fu[1], Xiao Lin[1](✉), Xinliang Feng[2,3](✉), Shixuan Du[1,5](✉), Hong-Jun Gao[1,5](✉)

[1] Beijing National Center for Condensed Matter Physics and Institute of Physics & University of Chinese Academy of Sciences, Chinese Academy of Sciences, Beijing 100190, PR China

[2] Center for Advancing Electronics Dresden (cfaed) & Faculty of Chemistry and Food Chemistry, Technische Universität Dresden, D-01069 Dresden, Germany

[3] Max Planck Institute of Microstructure Physics, Weinberg 2, Halle, 06120 Germany

[4] Department of Chemistry, State Key Laboratory of Synthetic Chemistry, The University of Hong Kong, Pokfulam Road, Hong Kong, China

[5] Songshan Lake Materials Laboratory, Dongguan, Guangdong 523808, PR China

[§] Xiao Chang, Li Huang, Yixuan Gao and Yubin Fu contributed equally to this work.

Nano Res., **Just Accepted Manuscript** • https://doi.org/10.1007/s12274-023-5605-2

http://www.thenanoresearch.com on Feb. 28, 2023

Just Accepted

Address correspondence to First A. Firstauthor, email1; Third C. Thirdauthor, email2

Xiao Chang[1, §], Li Huang[1, §], Yixuan Gao[1, §], Yubin Fu[2, §], Ji Ma[2, 3], Huan Yang[1], Junzhi Liu[4], Xiaoshuai Fu[1], Xiao Lin(✉)[1], Xinliang Feng(✉)[2, 3], Shixuan Du(✉)[1, 5] and Hong-Jun Gao(✉)[1, 5]

[1] Beijing National Center for Condensed Matter Physics and Institute of Physics & University of Chinese Academy of Sciences, Chinese Academy of Sciences, Beijing 100190, PR China

[2] Center for Advancing Electronics Dresden (*cfaed*) & Faculty of Chemistry and Food Chemistry, Technische Universität Dresden, D-01069 Dresden, Germany

[3] Max Planck Institute of Microstructure Physics, Weinberg 2, Halle, 06120 Germany

[4] Department of Chemistry, State Key Laboratory of Synthetic Chemistry, The University of Hong Kong, Pokfulam Road, Hong Kong, China

[5] Songshan Lake Materials Laboratory, Dongguan, Guangdong 523808, PR China

[§] Xiao Chang, Li Huang, Yixuan Gao and Yubin Fu contributed equally to this work.

(✉)Address correspondence to Hong-Jun Gao, hjgao@iphy.ac.cn; Shixuan Du, sxdu@iphy.ac.cn; Xinliang Feng, xinliang.feng@tu-dresden.de; Xiao Lin, xlin@ucas.ac.cn

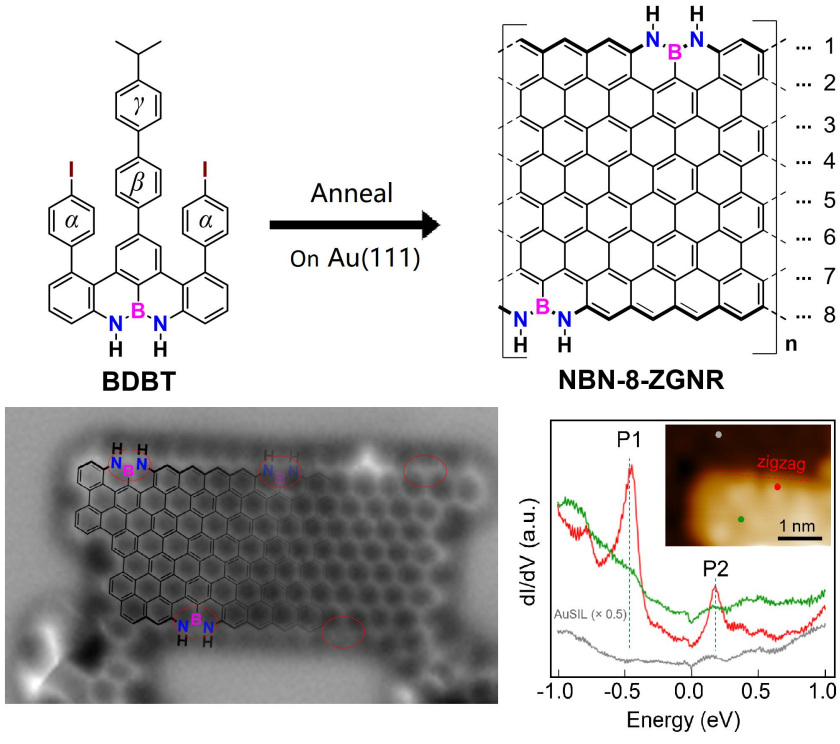

Observation of edge states of NBN-doped zigzag graphene nanoribbons.

Nano Research

ISSN 1998-0124 CN 11-5974/O4
https://doi.org/(automatically inserted by the publisher)

Research Article

On-surface synthesis and edge states of NBN-doped zigzag graphene nanoribbons

Xiao Chang[1, §], Li Huang[1, §], Yixuan Gao[1, §], Yubin Fu[2, §], Ji Ma[2, 3], Huan Yang[1], Junzhi Liu[4], Xiaoshuai Fu[1], Xiao Lin (✉)[1] Xinliang Feng (✉)[2, 3], Shixuan Du (✉)[1, 5] and Hong-Jun Gao (✉)[1, 5]

[1] *Beijing National Center for Condensed Matter Physics and Institute of Physics & University of Chinese Academy of Sciences, Chinese Academy of Sciences, Beijing 100190, PR China*
[2] *Center for Advancing Electronics Dresden (cfaed) & Faculty of Chemistry and Food Chemistry, Technische Universität Dresden, D-01069 Dresden, Germany*
[3] *Max Planck Institute of Microstructure Physics, Weinberg 2, Halle, 06120 Germany*
[4] *Department of Chemistry, State Key Laboratory of Synthetic Chemistry, The University of Hong Kong, Pokfulam Road, Hong Kong, China*
[5] *Songshan Lake Materials Laboratory, Dongguan, Guangdong 523808, PR China*
[§] *Xiao Chang, Li Huang, Yixuan Gao and Yubin Fu contributed equally to this work.*

Received: day month year / **Revised:** day month year / **Accepted:** day month year (automatically inserted by the publisher)

ABSTRACT

Zigzag graphene nanoribbons (ZGNRs) with spin-polarized edge states have potential applications in carbon-based spintronics. The electronic structure of ZGNRs can be effectively tuned by different widths or dopants, which require delicately designed monomers. Here, we report the successful synthesis of ZGNR with a width of eight carbon zigzag lines and nitrogen-boron-nitrogen (NBN) motifs decorated along the zigzag edges (NBN-8-ZGNRs) on Au(111) surface, which starts from a specially designed U-shaped monomer with preinstalled NBN units at the zigzag edge. Chemical-bond-resolved non-contact atomic force microscopy imaging confirms the zigzag-terminated edges and the existence of NBN dopants. The electronic states distributed along the zigzag edges have been revealed after a silicon-layer intercalation at the interface of NBN-8-ZGNR and Au(111). Our work enriches the ZGNR family with a new dopant and larger width, which provides more candidates for future carbon-based nanoelectronic and spintronic applications.

KEYWORDS

zigzag graphene nanoribbons, NBN dopant, edge states, STM, nc-AFM, DFT calculations

1 Introduction

Graphene nanoribbons (GNRs) are renowned for their fascinating electronic and magnetic properties, which have potential applications in carbon-based nanoelectronics and spintronics.[1] The edge configurations of GNRs greatly influence their electronic structures,[2] thus atomically precise synthetic methods are needed to construct GNRs with designed properties. Surface-assistant fabrication starting with organic precursors has been proven to be a powerful bottom-up approach to synthesize specifically designed graphene nanostructures.[3-10] Up to now, a variety of GNRs have been synthesized on surface, including GNRs with armchair-,[9, 11-13] zigzag-,[4, 14] and chevron-terminated edges,[15-17] with dopants of nitrogen,[18, 19] boron,[11-13, 20] and sulfur atoms,[15, 21, 22] and heterostructures splicing with different width[6-8, 23, 24] or edges[25-27].

Zigzag GNRs (ZGNRs) host spin-polarized electronic edge states[2], which is an ideal prototype material to explore carbon-based spintronics and qubits.[28-30] The spin-polarized edge states are anti-ferromagnetic on opposite edges of ZGNRs, which, however, is difficult to be directly observed due to a strong hybridization with the underlying metal substrate.[4] Moreover, the zigzag edges constructed with all carbon atoms are highly reactive,[31, 32] further hindering their further exploration. An effective strategy to decouple the zigzag edges from the substrate is to introduce a superlattice of isoelectronic dopants along the edges, such as nitrogen (N) atoms and nitrogen-boron-nitrogen (NBN) motifs.[14, 33] A N-doped 6-ZGNR was recently demonstrated to successfully stabilize the edges and electronically decouple the spin-polarized edge states from hybridization with the substrate.[14] The NBN dopants have been predicted not only to have the ability to stabilize the edges,[34] but also to enable the formation of radical cation by selective oxidation,[35] which is the isoelectronic structure of its all-carbon skeleton with an open-shell character. NBN-doped partial ZGNRs with cove features were synthesized in 2020 by us,[33] in which the spin-polarized edge states are absent due to the short length of continuous zigzag edges. Therefore, to investigate the spin-polarized electronic edge states, a full ZGNR with NBN-doped superlattice along the edges will be a potential candidate.

Address correspondence to Hong-Jun Gao, hjgao@iphy.ac.cn; Shixuan Du, sxdu@iphy.ac.cn; Xinliang Feng, xinliang.feng@tu-dresden.de; Xiao Lin xlin@ucas.ac.cn

Here, we design and synthesize a U-shaped precursor with an interior isopropyl-diphenyl group, 4,13-bis(4-iodophenyl)-2-(4'-isopropyl-[1,1'-biphenyl]-4-yl)-8 H,9H-8,9-diaza-8a-borabenzo[fg]tetracene (**BDBT** shown in Fig. 1(a)), which will yield ZGNRs with eight carbon zigzag lines in width and NBN motifs along the edges (NBN-8-ZGNR). Subsequent deposition of **BDBT** molecules on Au(111) surface followed by annealing demonstrates the formation of NBN-8-ZGNRs. Using nc-AFM, we confirm the structures of the NBN-8-ZGNRs and their purely zigzag edges. By silicon intercalation,[36-38] a gold silicide (AuSIL) buffer layer[39] is created between Au and NBN-ZGNRs, which effectively decouple the surface states of Au(111) and enable the measurement of the electronic states of the NBN-ZGNRs. Localized states are detected on the zigzag edges, which indicates the edge states are preserved on NBN-doped zigzag edges. Furthermore, the detection of the edge states demonstrates that NBN dopants make the zigzag edges less active and survive during the silicon intercalation process.

2 Result and discussion

The U-shaped **BDBT** monomer, which has a NBN-containing benzotetracene core with additional α, β and γ benzene rings, an isopropyl group and two halogen functions (Fig. 1(a)), was successfully obtained through multi-step solution-based chemical reactions as displayed in Scheme 1. Firstly, by Suzuki reaction of (4-isopropylphenyl)boronic acid **(1)** with (4-bromophenyl)trimethylsilane, (4'-isopropyl-[1,1'-biphenyl]-4-yl)trimethylsilane **(2)** was obtained in 96% yield. Next, the trimethylsilyl (TMS) group in compound **2** was converted into boronic acid group by treatment with an excess of boron tribromide (BBr_3) followed by H_2O, which gave the (4'-isopropyl-[1,1'-biphenyl]-4-yl)boronic acid **(3)** in 88% yield. Then a Suzuki reaction of compound **3** with 1,3-dibromo-5-iodobenzene afforded 3,5-dibromo-4''-isopropyl-1,1':4',1''-terphenyl **(4)** in 91% yield. Afterward, 2,2'-(4''-isopropyl-[1,1':4',1''-terphenyl]-3,5-diyl)bis(4,4,5,5-tetramethyl-1,3,2-dioxaborolane) **(5)** was generated in 73% yield via the Miyaura borylation reaction based on **4**. A two-fold Suzuki reaction of compound **5** with 1-bromo-2-iodo-3-nitrobenzene afforded 2-bromo-5'-(2-bromo-6-nitrophenyl)-4'''-isopropyl-6-nitro-1,1':3',1'':4'',1'''-quaterphenyl **(6)** in 58% yield. After another two-fold Suzuki reaction based on compound **6** and (4-(trimethylsilyl)phenyl)boronic acid, (5''-(4'-isopropyl-[1,1'-biphenyl]-4-yl)-3',6'''-dinitro-[1,1':2',1'':3'',1''':2''',1''''-quinquephenyl]-4,4''''-diyl)bis(trimethylsilane) **(7)** was synthezied in 84% yield. Next, the TMS groups in compound **7** were converted into iodo groups by treatment with an excess of ICl, giving 4,4''''-diiodo-5''-(4'-isopropyl-[1,1'-biphenyl]-4-yl)-3',6'''-dinitro-1,1':2',1'':3'',1''':2''',1''''-quinquephenyl **(8)** in 50% yield. Subsequently, compound **8** was reduced to 4,4''''-diiodo-5''-(4'-isopropyl-[1,1'-biphenyl]-4-yl)-[1,1':2',1'':3'',1''':2''',1''''-quinquephenyl]-3',6'''-diamine **(9)** at room temperature in the presence of hydrogen gas with Pt/C in quantitative yield. Finally, heating of a solution of compound **9** in *o*-DCB at 180 °C in the presence of BBr_3 with an excess of NEt_3 gave **BDBT** in 33% yield. The structure of **BDBT** was unambiguously confirmed by the NMR spectroscopy (Fig. S24-28 in the Electronic Supplementary Material (ESM)) and HR-MALDI-TOF mass spectrometry (Fig. S29 in the ESM) after purification by silica column chromatography and subsequent recrystallization in $CHCl_3$/MeOH.

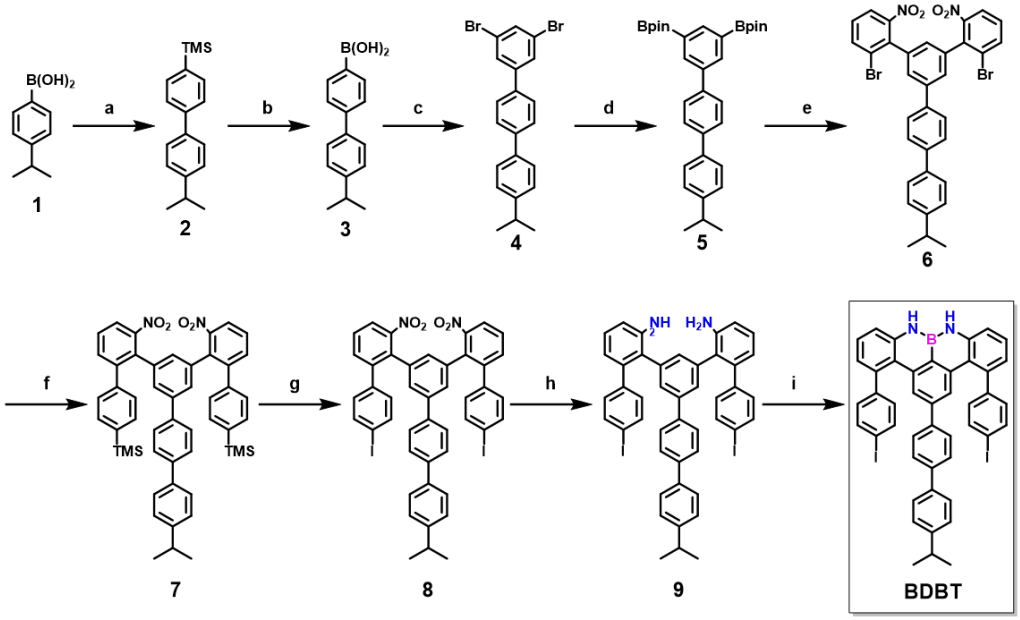

Scheme 1 Synthetic route to **BDBT**. Reagents and conditions: (a) (4-bromophenyl)trimethylsilane, $Pd(PPh_3)_4$, Cs_2CO_3, toluene, EtOH, H_2O, 80 °C, 12 h, 96%; (b) BBr3, 100 °C, 4 h, then H_2O, n-hexane, 0 °C, 4 h, 88%; (c) 1,3-dibromo-5-iodobenzene, $Pd(PPh_3)_4$, Cs_2CO_3, toluene, EtOH, H2O, 80 °C, 12 h, 91%; (d) bis(pinacolato)diboron, $Pd(dppf)Cl_2$, KOAc, DMSO, 100 °C, 24 h, 73%; e) 1-bromo-2-iodo-3-nitrobenzene, Pd(dppf)Cl2, Na_2CO_3, THF, H2O, 70 °C, 12 h, 58%; (f) (4-(trimethylsilyl)phenyl)boronic acid, $Pd(PPh_3)_4$, Cs_2CO_3, toluene, EtOH, H_2O, 80 °C, 12 h, 84%; (g) ICl, DCM, 0 °C - r.t., 12 h, 50%; (h) MeOH/THF, Pt/C, H_2, r.t., 12 h, quantitative yield (crude); i) BCl3, NEt_3, *o*-DCB, 180 °C, 12 h, 30%.

Nano Research

ISSN 1998-0124 CN 11-5974/O4

https://doi.org/(automatically inserted by the publisher)

Starting from the **BDBT** monomer, the surface-assisted polymerization and subsequent cyclization enable the synthesis of NBN-8-ZGNRs on Au(111), as illustrated in Fig. 1(a). On the zigzag edges of NBN-8-ZGNRs, the NBN motifs insert in every six benzene rings, forming a superlattice of substitutional dopants along both edges. Density functional theory (DFT) calculations reveal that the NBN-8-ZGNRs, like other GNRs with zigzag edge topologies, have edge states that couple ferromagnetically along each edge and antiferromagnetically between the opposite edges (Fig. 1(b)). The spin-polarized edge states mainly distribute on the edge carbon atoms, but have little contribution from the substitutional dopants of NBN motifs. The projected density of states (PDOS) of the two edges are displayed in the upper and lower part of Fig. 1(c) respectively. They are the density of states projected to the upper (lower) edge atoms as marked by the black dashed boxes in Fig. 1(b), which clearly demonstrate the spin-polarized nature of the edges. The DFT calculated band structure of a freestanding NBN-8-ZGNR in Fig. 1(d) shows that this ribbon has an indirect band gap of 0.27 eV, and the spin up and down states are degenerate in the ribbon.

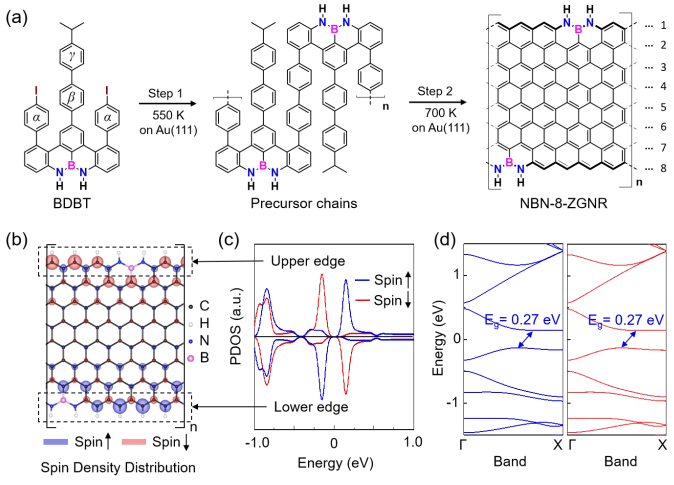

Figure 1 Synthetic process, DFT calculated band structure and spatial distribution of spin-ordered edge states of NBN-8-ZGNRs. (a) Monomer **BDBT**, a U-shape monomer with an additional isopropyl-diphenyl group in the interior, is designed to synthesize NBN-8-ZGNRs through polymerization (step 1) and subsequent cyclodehydrogenation (step 2) on Au(111) surface. (b) DFT calculated spatial distribution of spin density in an NBN-8-ZGNR, in which the blue and coral circles denote the spin up and spin down states. (c) PDOS of the upper edge and lower edge atoms as marked by the black dashed boxes in (b). The blue and red lines indicate the spin up and spin down states. (d) DFT calculated band structure of a freestanding NBN-8-ZGNR. The blue and red lines indicate the spin up and spin down channels. The spin up and spin down states are degenerate.

The **BDBT** monomer was sublimed from a molecule cell evaporator at 530 K onto a clean Au(111) substrate held at room temperature in ultrahigh vacuum. The as-deposited monomers form linear or circular self-assemblies that adsorb respectively on the *fcc* and elbow region of the Au(111) surface, as shown in Fig. 2(a). After annealing at 550 K, the monomers went through dehalogenation and C-C coupling to form linear precursor chains as displayed in Fig. 2(b). However, in the zoomed-in image in Fig. 2(c), the precursor chains are clearly resolved to be made of short segments as denoted by the red boxes. The chevron stripes are the polymerized backbones, and the bright dots are rotated benzene rings that connect to the backbone with C-C single bonds. Statistics on the length distribution in Fig. 2(g) (Fig. S30 in the ESM) display that most precursor chains consist of 2-5 monomers. The limited lengths in this case are most likely due to the steric hindrance imposed by the rotated benzene rings, which prevent the radical addition reactions even though the monomers seem to be close enough.

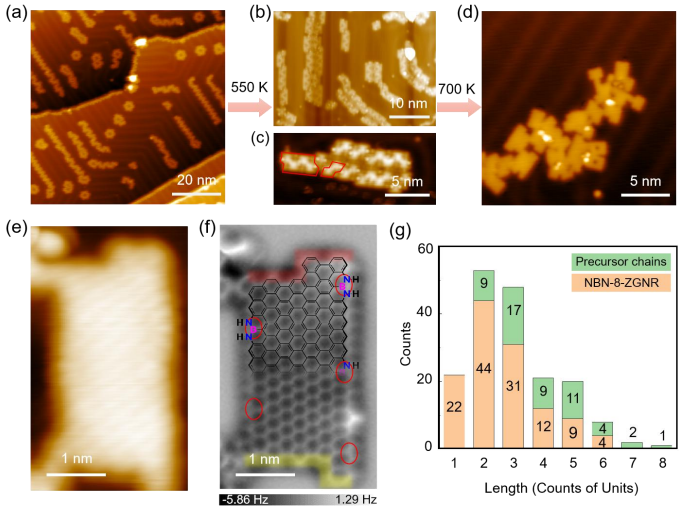

Figure 2 Bottom-up synthesis and characterization of NBN-8-ZGNRs on Au(111). (a) Large-scale STM image of as-deposited **BDBT** monomers on Au(111). (V_s = -1 V, I_t = 30 pA) (b) Large-scale STM image of precursor chains formed after annealing the sample at 550K. (V_s = -1 V, I_t = 30 pA) (c) High-resolution zoomed-in STM image of the polymers, in which two oligomers are marked by red boxes. (V_s = 100 mV, I_t = 50 pA) (d) Large-scale STM image of fully cyclized NBN-8-ZGNRs after annealing the polymers at 700 K. (V_s = -200 mV, I_t = 10 pA) (e) Zoomed-in STM image of an NBN-8-ZGNR. (V_s = -200 mV, I_t = 40 pA) (f) Constant-height nc-AFM frequency shift image of the ribbon in (e) taken with a CO-functionalized tip. The chemical structure is superimposed on the upper part of the ribbon. The red ovals denote the position of the NBN motifs. The red and yellow shades denote the upper and lower edges mentioned in the manuscript, respectively. (g) Statistics of the length distribution of the precursor chains (green) and NBN-8-ZGNRs (orange) after annealing at 700 K.

After further annealing at 700 K, the precursor chains were fully cyclized to form NBN-8-ZGNRs. As shown in Fig. 2(d), most NBN-8-ZGNRs are connected into a branched structure, indicating there were side reactions at 700 K. These side reactions, along with the short precursor backbones yielded in the last step, resulting in GNRs comprised of few units. Statistics of the length distribution (Fig. 2(g), Fig. S31 in the ESM) show that about 62% of the products are segments composed of 2 or 3 monomers, while about 18% of them are still monomers. In order to distinguish the boundaries between one-dimensional GNRs and zero-dimensional nanographenes

in the products, we used DFT calculated energy gap as a criterion. The calculated DOS of NBN-8-ZGNR segments with increasing number of units reveal that the energy gap decreases with increasing lengths (Fig. S33). The energy gap of a tetramer (0.29 eV) is comparable to that of infinite GNR (0.27 eV). Therefore, the nanostructures with more than four monomers can be considered as one-dimensional NBN-8-ZGNRs.

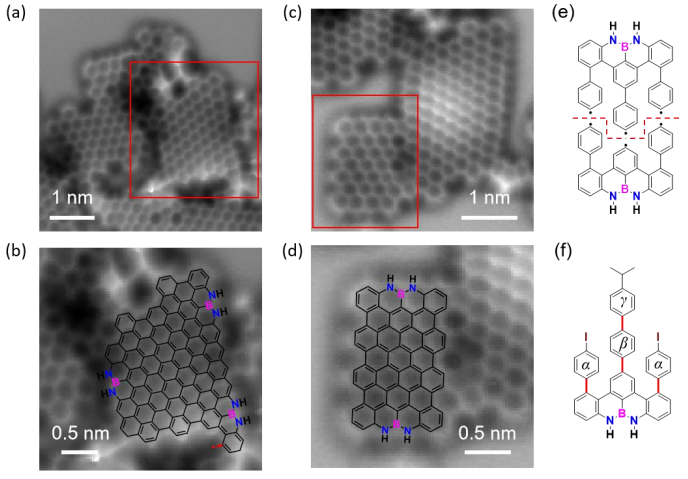

Figure 3 nc-AFM images of several NBN-8-ZGNR segments. (a) and (c) Constant-height AFM frequency shift images of two NBN-8-ZGNR segments. (b) and (d) Zoomed-in images of the red boxes in (a) and (c), respectively, overlayed with chemical structures. The benzene ring in red in (b) signifies the cleavage of an α benzene ring at the terminus. (e) Chemical structures of two monomers in which the C-C bond connecting the β or γ benzene rings is cleaved. The two monomers are separated by a red dashed line. (f) The **BDBT** molecule structure with the C-C bonds that are most likely to dissociate at elevated temperature labelled in red.

Fig. 2(e) displays an NBN-8-ZGNR consisting of 5 monomers. To precisely resolve its structure, we performed nc-AFM imaging in the same area of Fig. 2(e), which clearly shows the zigzag edges. Starting from one terminus of the GNR, we are able to identify the monomers that made up the GNR, as marked by T-shaped boxes in Fig. S34(a). By comparing the atoms along the zigzag edges with those in the **BDBT** monomer, i.e., the atoms with the same number labels in Fig. S34(a) and (b), the NBN motifs can be located along the zigzag edges of NBN-8-GNRs. Superimposed with the chemical structure, the NBN motifs are clearly located along the edges, as indicated by the red ovals in Fig. 2(f). Note that there is a bright protrusion at the lower part of the right edge, which, judging from the chemical structure, is a H_2 defect that is commonly seen in ZGNR edges when using precursors with methyl groups.[4]

The two termini of the NBN-8-ZGNR in Fig. 2(f) have different morphologies. The upper terminus (in red shade in Fig. 2(f)) has two protruded benzene rings in the armchair direction, indicating the terminal monomer has not connected with another monomer after dehalogenation. The lower terminus (in yellow shade in Fig. 2(f)) only has one extra benzene ring extending from an armchair ending, which is yielded by the detachment of the α benzene ring. To further understand the termini structures and possible cleavage of bonds during the growth of NBN-8-ZGNRs, more chemical-bond resolved nc-AFM images were obtained, as shown in Fig. 3. In Fig. 3(a) and (b), the same termini are found as those in Fig. 2(f), indicating the detachment of the α benzene ring is easy in the reaction process. The patch in the red box in Fig. 3(c) is another commonly seen structure on the surface. The zoomed-in image in Fig. 3(d) with chemical structure overlayed indicates that this patch is formed by two monomers fused head-to-head, with both β and γ benzene rings cleaved in one monomer and only β benzene ring cleaved in the other, as plotted in Fig. 3(e). From the nc-AFM images, we confirm that the C-C single bonds that connect the α, β and γ benzene rings are likely to be cleaved during cyclodehydrogenation, as shown in Fig. 3(f) labeled in red, which could be the main reason for the short length and cross-linked structures of the resulting NBN-8-ZGNRs. Since most precursor chains still contain the α, β and γ benzene rings as shown in Fig. 2(c), the detachment of these benzene rings should happen at the annealing process of 700 K.

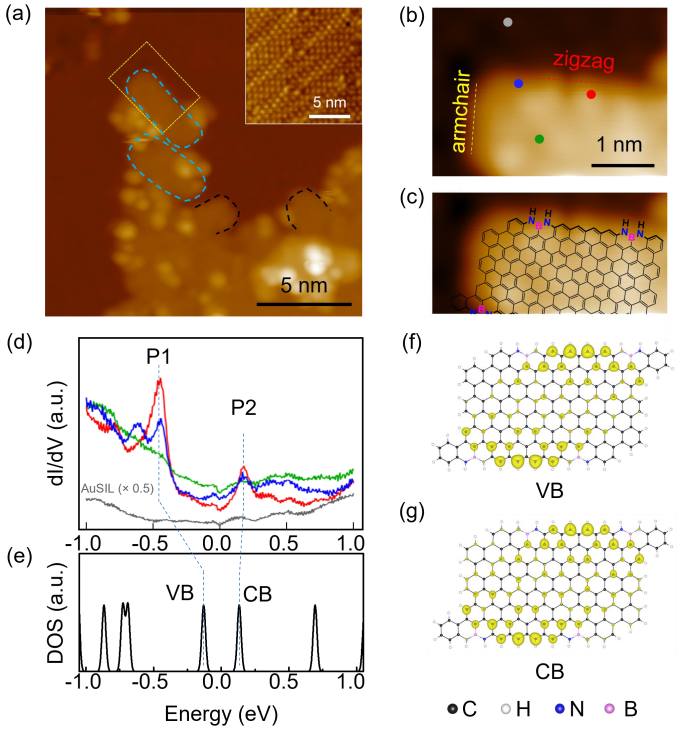

Figure 4 Edge-states characterization of NBN-8-ZGNRs on the Si intercalated Au(111) substrate. (a) Large-scale STM image of NBN-8-ZGNRs on AuSIL/Au(111) (Vs = -1 V, It = 50 pA). Blue and black dashed lines indicate the NBN-8-ZGNR segments on AuSIL. The inset is a high-resolution STM image of the AuSIL surface (Vs = -1 V, It = 500 pA). (b) Zoomed-in STM image of the ribbon in the yellow box of (a) (Vs = -1 V, It = 50 pA). The red and yellow dashed lines indicate the zigzag and armchair edges of the ribbon. The gray, red, blue and green dots denote the positions where dI/dV spectra in (d) were performed. (c) Chemical structure superimposed on the same ribbon in (b). (d) dI/dV spectra obtained on AuSIL substrate (grey), GNR zigzag edge (red and blue) and GNR interior (green) (Vs = -1 V, It = 1 nA before opening feedback loop, frequency = 931 Hz, Vmod = 5 mV). (e)-(g) DFT calculated DOS (e) and spatial distribution of local DOS at VB (f) and CB (g) of a free-standing NBN-8-ZGNR segment.

Similar to the case of 6-ZGNRs, there is a strong electronic

coupling between NBN-8-ZGNRs and Au(111) surface that suppresses the intrinsic electronic states of the ribbons. As displayed in Fig. S32 in the ESM, the dI/dV spectra taken on the edges and in the middle of the ribbon are all dominated by the surface states of the gold substrate. In order to decouple the surface states of Au(111), we deposited silicon on the sample held at 550 K, which leads to the formation of a gold silicide (AuSIL) layer on the surface of Au(111), as shown by the inset of Fig. 4(a). The AuSIL strongly changed the morphology of Au(111), on which the herringbone reconstruction transforms to a flat surface. Furthermore, some of the silicon atoms diffuse underneath the ribbons through their edges, which intercalates the AuSIL buffer layer at the interface of NBN-8-GNR/Au(111). However, the silicon intercalation also induces contaminations on the NBN-8-GNRs, such as residual silicon clusters at the ribbon edges, and small silicon (or AuSIL) islands that fill in the interspace of the cross-linked ribbons. The latter case makes it difficult to distinguish the terminus of some ribbons (the black dashed curves in Fig. 4(a)). In addition, the termini of the ribbons seem to be modified by silicon intercalation, transforming the corners between the zigzag and the armchair edges from sharp corners to round corners, as marked by the blue dashed shapes in Fig. 4(a). These modifications indicate that some parts of the ribbons, such as the termini, may be buried under the AuSIL layer.

Fig. 4(b) displays a zoomed-in topography of the ribbon in the yellow box in Fig. 4(a). The zigzag edge and the armchair terminus are indicated by red and yellow dashed lines, respectively. Due to the Si clusters attached to one of the edges, Fig. 4(b) only shows the clean zigzag edge of the ribbon. The most likely chemical structure of this ribbon is superimposed in Fig. 4(c). We performed dI/dV spectra on the zigzag edge (the red and blue dots in Fig. 4(b)) and the interior of the ribbon (the green dot), and the corresponding spectra are shown in Fig. 4(d) in the same color code. The spectrum at the interior of the ribbon nearly mimics that on the AuSIL (the grey spectrum in Fig. 4(d)), only that the density of the occupied states is higher than the unoccupied states. For the spectrum at the edge, however, prominent electronic states are observed around Fermi level at -450 mV and 180 mV, as denoted by P1 and P2 in Fig.4(d), respectively. DFT calculated DOS on the free-standing model of the structure in Fig. 4(c) exhibits two states around the Fermi level, which can be attributed to the valence band (VB) and conduction band (CB), as displayed in Fig. 4(e). Fig. 4(f) and (g) demonstrate the spatial distribution of the calculated local DOS at VB and CB, which mainly disperse along the zigzag edges and decay in the interior of the GNR, having the same distribution as the P1 and P2 states obtained in dI/dV spectra. These results indicate that the electronic states along the edges exist in NBN-8-ZGNRs, and the introduction of the NBN dopants preserves these states and stabilizes the zigzag edges to survive the formation of the AuSIL bufferlayer.

3 Conclusions

In conclusion, we have synthesized NBN-8-ZGNRs on Au(111) substrate starting from a specially designed monomer **BDBT**. Nc-AFM images confirm the successful introduction of a NBN dopant superlattice along the zigzag edges, and reveal that the additional benzene rings are easy to detach from the NBN core, which results in short segments of NBN-8-ZGNRs. After the formation of AuSIL bufferlayer, the ribbons are electronically decoupled from the substrate, enabling us to detect the edge states. Our work provides a new ribbon with NBN dopants and a larger width in the ZGNR toolbox compared with the existing ones, and reveals that the zigzag edges in NBN-8-ZGNRs are robust enough to survive the formation of AuSIL at the ZGNR-Au(111) interface.

Acknowledgements

The work is supported by grants from the National Key Research and Development Projects of China (2019YFA0308500), the National Natural Science Foundation of China (61888102), the Chinese Academy of Sciences (XDB30000000, YSBR-003), the EU Graphene Flagship (Graphene Core 3, 881603), H2020-MSCA-ITN (ULTIMATE, No. 813036), the Center for Advancing Electronics Dresden (cfaed), H2020-EU.1.2.2.- FET Proactive Grant (LIGHT-CAP, 101017821) and the DFG-SNSF Joint Switzerland-German Research Project (EnhanTopo, No. 429265950).

Electronic Supplementary Material: Supplementary material (additional information on precursor synthesis route, NMR spectrum and mass spectroscopy measurements, GNR statistics based on STM images) is available in the online version of this article at http://dx.doi.org/10.1007/s12274-***-****-* (automatically inserted by the publisher).

References

[1] Han, W.;Kawakami, R. K.;Gmitra, M.; Fabian, J. Graphene spintronics. *Nat. Nanotechnol.* **2014**, *9*, 794-807.

[2] Nakada, K.;Fujita, M.;Dresselhaus, G.; Dresselhaus, M. S. Edge state in graphene ribbons: Nanometer size effect and edge shape dependence. *Phys. Rev. B* **1996**, *54*, 17954-17961.

[3] Han, P.;Akagi, K.;Federici Canova, F.;Mutoh, H.;Shiraki, S.;Iwaya, K.;Weiss, P. S.;Asao, N.; Hitosugi, T. Bottom-Up Graphene-Nanoribbon Fabrication Reveals Chiral Edges and Enantioselectivity. *ACS Nano* **2014**, *8*, 9181-9187.

[4] Ruffieux, P.;Wang, S.;Yang, B.;Sánchez-Sánchez, C.;Liu, J.;Dienel, T.;Talirz, L.;Shinde, P.;Pignedoli, C. A.;Passerone, D.;Dumslaff, T.;Feng, X.;Müllen, K.; Fasel, R. On-surface synthesis of graphene nanoribbons with zigzag edge topology. *Nature* **2016**, *531*, 489-492.

[5] Talirz, L.;Söde, H.;Dumslaff, T.;Wang, S.;Sanchez-Valencia, J. R.;Liu, J.;Shinde, P.;Pignedoli, C. A.;Liang, L.;Meunier, V.;Plumb, N. C.;Shi, M.;Feng, X.;Narita, A.;Müllen, K.;Fasel, R.; Ruffieux, P. On-Surface Synthesis and Characterization of 9-Atom Wide Armchair Graphene Nanoribbons. *ACS Nano* **2017**, *11*, 1380-1388.

[6] Gröning, O.;Wang, S.;Yao, X.;Pignedoli, C. A.;Borin Barin, G.;Daniels, C.;Cupo, A.;Meunier, V.;Feng, X.;Narita, A.;Müllen, K.;Ruffieux, P.; Fasel, R. Engineering of robust topological quantum phases in graphene nanoribbons. *Nature* **2018**, *560*, 209-213.

[7] Rizzo, D. J.;Veber, G.;Cao, T.;Bronner, C.;Chen, T.;Zhao, F.;Rodriguez, H.;Louie, S. G.;Crommie, M. F.; Fischer, F. R. Topological band engineering of graphene nanoribbons. *Nature* **2018**, *560*, 204-208.

[8] Rizzo, D. J.;Veber, G.;Jiang, J.;McCurdy, R.;Cao, T.;Bronner, C.;Chen, T.;Louie, S. G.;Fischer, F. R.; Crommie, M. F. Inducing metallicity in graphene nanoribbons via zero-mode superlattices. *Science* **2020**, *369*, 1597-1603.

[9] Cai, J.;Ruffieux, P.;Jaafar, R.;Bieri, M.;Braun, T.;Blankenburg, S.;Muoth, M.;Seitsonen, A. P.;Saleh, M.;Feng, X.;Müllen, K.; Fasel, R. Atomically precise bottom-up fabrication of graphene nanoribbons. *Nature* **2010**, *466*, 470-473.

[10] Liu, J.;Li, B.-W.;Tan, Y.-Z.;Giannakopoulos, A.;Sanchez-Sanchez, C.;Beljonne, D.;Ruffieux, P.;Fasel, R.;Feng, X.; Müllen, K. Toward Cove-Edged Low Band Gap Graphene Nanoribbons. *J. Am. Chem. Soc.* **2015**, *137*, 6097-6103.

[11] Senkovskiy, B. V.;Usachov, D. Y.;Fedorov, A. V.;Marangoni, T.;Haberer, D.;Tresca, C.;Profeta, G.;Caciuc, V.;Tsukamoto, S.;Atodiresei, N.;Ehlen, N.;Chen, C.;Avila, J.;Asensio, M. C.;Varykhalov, A. Y.;Nefedov, A.;Wöll, C.;Kim, T. K.;Hoesch, M.;Fischer, F. R.; Grüneis, A. Boron-Doped Graphene Nanoribbons: Electronic Structure and Raman Fingerprint. *ACS Nano* **2018**, *12*, 7571-7582.

[12] Sun, K.;Silveira, O. J.;Saito, S.;Sagisaka, K.;Yamaguchi, S.;Foster, A. S.; Kawai, S. Manipulation of Spin Polarization in Boron-Substituted Graphene Nanoribbons. *ACS Nano* **2022**, 10.1021/acsnano.2c04563.

[13] Cloke, R. R.;Marangoni, T.;Nguyen, G. D.;Joshi, T.;Rizzo, D. J.;Bronner, C.;Cao, T.;Louie, S. G.;Crommie, M. F.; Fischer, F. R. Site-Specific Substitutional Boron Doping of Semiconducting Armchair Graphene Nanoribbons. *J. Am. Chem. Soc.* **2015**, *137*, 8872-8875.

[14] Blackwell, R. E.;Zhao, F.;Brooks, E.;Zhu, J.;Piskun, I.;Wang, S.;Delgado, A.;Lee, Y.-L.;Louie, S. G.; Fischer, F. R. Spin splitting of dopant edge state in magnetic zigzag graphene nanoribbons. *Nature* **2021**, *600*, 647-652.

[15] Cao, Y.;Qi, J.;Zhang, Y.-F.;Huang, L.;Zheng, Q.;Lin, X.;Cheng, Z.;Zhang, Y.-Y.;Feng, X.;Du, S.;Pantelides, S. T.; Gao, H.-J. Tuning the morphology of chevron-type graphene nanoribbons by choice of annealing temperature. *Nano Res.* **2018**, *11*, 6190-6196.

[16] Liu, J.;Li, B.-W.;Tan, Y.-Z.;Giannakopoulos, A.;Sanchez-Sanchez, C.;Beljonne, D.; Ru, P. Toward Cove-Edged Low Band Gap Graphene Nanoribbons. *J. Am. Chem. Soc.* **2015**, 7.

[17] Cai, J.;Pignedoli, C. A.;Talirz, L.;Ruffieux, P.;Söde, H.;Liang, L.;Meunier, V.;Berger, R.;Li, R.;Feng, X.;Müllen, K.; Fasel, R. Graphene nanoribbon heterojunctions. *Nat. Nanotechnol.* **2014**, *9*, 896-900.

[18] Pawlak, R.;Liu, X.;Ninova, S.;D'Astolfo, P.;Drechsel, C.;Sangtarash, S.;Häner, R.;Decurtins, S.;Sadeghi, H.;Lambert, C. J.;Aschauer, U.;Liu, S.-X.; Meyer, E. Bottom-up Synthesis of Nitrogen-Doped Porous Graphene Nanoribbons. *J. Am. Chem. Soc.* **2020**, *142*, 12568-12573.

[19] Wen, E. C. H.;Jacobse, P. H.;Jiang, J.;Wang, Z.;McCurdy, R. D.;Louie, S. G.;Crommie, M. F.; Fischer, F. R. Magnetic Interactions in Substitutional Core-Doped Graphene Nanoribbons. *J. Am. Chem. Soc.* **2022**, *144*, 13696-13703.

[20] Kawai, S.;Saito, S.;Osumi, S.;Yamaguchi, S.;Foster, A. S.;Spijker, P.; Meyer, E. Atomically controlled substitutional boron-doping of graphene nanoribbons. *Nat. Commun.* **2015**, *6*, 8098.

[21] Yang, H.;Gao, Y.;Niu, W.;Chang, X.;Huang, L.;Liu, J.;Mai, Y.;Feng, X.;Du, S.; Gao, H.-J. Fabrication of sulfur-doped cove-edged graphene nanoribbons on Au(111)\ast. *Chin. Phys. B* **2021**, *30*, 077306.

[22] Nguyen, G. D.;Toma, F. M.;Cao, T.;Pedramrazi, Z.;Chen, C.;Rizzo, D. J.;Joshi, T.;Bronner, C.;Chen, Y.-C.;Favaro, M.;Louie, S. G.;Fischer, F. R.; Crommie, M. F. Bottom-Up Synthesis of $N = 13$ Sulfur-Doped Graphene Nanoribbons. *J. Phys. Chem. C* **2016**, *120*, 2684-2687.

[23] Chen, Y.-C.;Cao, T.;Chen, C.;Pedramrazi, Z.;Haberer, D.;De Oteyza, D. G.;Fischer, F. R.;Louie, S. G.; Crommie, M. F. Molecular bandgap engineering of bottom-up synthesized graphene nanoribbon heterojunctions. *Nat. Nanotechnol.* **2015**, *10*, 156-160.

[24] Senkovskiy, B. V.;Nenashev, A. V.;Alavi, S. K.;Falke, Y.;Hell, M.;Bampoulis, P.;Rybkovskiy, D. V.;Usachov, D. Y.;Fedorov, A. V.;Chernov, A. I.;Gebhard, F.;Meerholz, K.;Hertel, D.;Arita, M.;Okuda, T.;Miyamoto, K.;Shimada, K.;Fischer, F. R.;Michely, T.;Baranovskii, S. D.;Lindfors, K.;Szkopek, T.; Grüneis, A. Tunneling current modulation in atomically precise graphene nanoribbon heterojunctions. *Nat. Commun.* **2021**, *12*, 2542.

[25] Rizzo, D. J.; Wu, M.; Tsai, H.-Z.; Marangoni, T.; Durr, R. A.; Omrani, A. A.; Liou, F.; Bronner, C.; Joshi, T.; Nguyen, G. D.; Rodgers, G. F.; Choi, W.-W.; Jørgensen, J. H.; Fischer, F. R.; Louie, S. G.; Crommie, M. F. Length-Dependent Evolution of Type II Heterojunctions in Bottom-Up-Synthesized Graphene Nanoribbons. *Nano Lett.* **2019**, 19 (5), 3221–3228.

[26] Nguyen, G. D.; Tsai, H.-Z.; Omrani, A. A.; Marangoni, T.; Wu, M.; Rizzo, D. J.; Rodgers, G. F.; Cloke, R. R.; Durr, R. A.; Sakai, Y.; Liou, F.; Aikawa, A. S.; Chelikowsky, J. R.; Louie, S. G.; Fischer, F. R.; Crommie, M. F. Atomically Precise Graphene Nanoribbon Heterojunctions from a Single Molecular Precursor. *Nat. Nanotechnol.* **2017**, 12 (11), 1077–1082.

[27] Li, J.; Sanz, S.; Merino-Díez, N.; Vilas-Varela, M.; Garcia-Lekue, A.; Corso, M.; de Oteyza, D. G.; Frederiksen, T.; Peña, D.; Pascual, J. I. Topological Phase Transition in Chiral Graphene Nanoribbons: From Edge Bands to End States. *Nat. Commun.* **2021**, 12 (1), 5538.

[28] Guo, G.-P.;Lin, Z.-R.;Tu, T.;Cao, G.;Li, X.-P.; Guo, G.-C. Quantum computation with graphene nanoribbon. *New J. Phys.* **2009**, *11*.

[29] Luis, F.; Coronado, E. Spinning on the edge of graphene. *Nature* **2018**, *557*, 645-647.

[30] Mandal, B.;Sarkar, S.;Pramanik, A.; Sarkar, P. Doped defective graphene nanoribbons: a new class of materials with novel spin filtering properties. *RSC Adv.* **2014**, *4*, 49946-49952.

[31] Berdonces-Layunta, A.;Lawrence, J.;Edalatmanesh, S.;Castro-Esteban, J.;Wang, T.;Mohammed, M. S. G.;Colazzo, L.;Peña, D.;Jelínek, P.; De Oteyza, D. G. Chemical Stability of (3,1)-Chiral Graphene Nanoribbons. *ACS Nano* **2021**, *15*, 5610-5617.

[32] Lawrence, J.;Berdonces-Layunta, A.;Edalatmanesh, S.;Castro-Esteban, J.;Wang, T.;Jimenez-Martin, A.;De La Torre, B.;Castrillo-Bodero, R.;Angulo-Portugal, P.;Mohammed, M. S. G.;Matěj, A.;Vilas-Varela, M.;Schiller, F.;Corso, M.;Jelinek, P.;Peña, D.; De Oteyza, D. G. Circumventing the stability problems of graphene nanoribbon zigzag edges. *Nature Chemistry* **2022**, 10.1038/s41557-022-01042-8.

[33] Fu, Y.;Yang, H.;Gao, Y.;Huang, L.;Berger, R.;Liu, J.;Lu, H.;Cheng, Z.;Du, S.;Gao, H.-J.; Feng, X. On-Surface Synthesis of NBN-Doped Zigzag-Edged Graphene Nanoribbons. *Angew. Chem.* **2020**, *132*, 8958-8964.

[34] Fu, Y.;Chang, X.;Yang, H.;Dmitrieva, E.;Gao, Y.;Ma, J.;Huang, L.;Liu, J.;Lu, H.;Cheng, Z.;Du, S.;Gao, H.-J.; Feng, X. NBN-Doped Bis-Tetracene and Peri-Tetracene: Synthesis and Characterization. *Angew. Chem. Int. Ed.* **2021**, *60*, 26115-26121.

[35] Wang, X.;Zhang, F.;Schellhammer, K. S.;Machata, P.;Ortmann, F.;Cuniberti, G.;Fu, Y.;Hunger, J.;Tang, R.;Popov, A. A.;Berger, R.;Müllen, K.; Feng, X. Synthesis of NBN-Type Zigzag-Edged Polycyclic Aromatic Hydrocarbons: 1,9-Diaza-9a-boraphenalene as a Structural Motif. *J. Am. Chem. Soc.* **2016**, *138*, 11606-11615.

[36] Mao, J.;Huang, L.;Pan, Y.;Gao, M.;He, J.;Zhou, H.;Guo, H.;Tian, Y.;Zou, Q.;Zhang, L.;Zhang, H.;Wang, Y.;Du, S.;Zhou, X.;Castro Neto, A. H.; Gao, H.-J. Silicon layer intercalation of centimeter-scale, epitaxially grown monolayer graphene on Ru(0001). *Appl. Phys. Lett.* **2012**, *100*, 093101.

[37] Li, G.;Zhou, H.;Pan, L.;Zhang, Y.;Huang, L.;Xu, W.;Du, S.;Ouyang, M.;Ferrari, A. C.; Gao, H.-J. Role of Cooperative Interactions in the Intercalation of Heteroatoms between Graphene and a Metal Substrate. *J. Am. Chem. Soc.* **2015**, *137*, 7099-7103.

[38] Guo, H.;Wang, X.;Huang, L.;Jin, X.;Yang, Z.;Zhou, Z.;Hu, H.;Zhang, Y.-Y.;Lu, H.;Zhang, Q.;Shen, C.;Lin, X.;Gu, L.;Dai, Q.;Bao, L.;Du, S.;Hofer, W.;Pantelides, S. T.; Gao, H.-J. Insulating SiO2 under Centimeter-Scale, Single-Crystal Graphene Enables Electronic-Device Fabrication. *Nano Letters* **2020**, *20*, 8584-8591.

[39] Deniz, O.;Sánchez-Sánchez, C.;Dumslaff, T.;Feng, X.;Narita, A.;Müllen, K.;Kharche, N.;Meunier, V.;Fasel, R.; Ruffieux, P. Revealing the Electronic Structure of Silicon Intercalated Armchair Graphene Nanoribbons by Scanning Tunneling Spectroscopy. *Nano Lett.* **2017**, *17*, 2197-2203.

TSINGHUA UNIVERSITY PRESS Springer

Electronic Supplementary Material

On-surface synthesis and edge states of NBN-doped zigzag graphene nanoribbons

Xiao Chang[1, §], Li Huang[1, §], Yixuan Gao[1, §], Yubin Fu[2, §], Ji Ma[2, 3], Huan Yang[1], Junzhi Liu[4], Xiaoshuai Fu[1], Xiao Lin[1, (✉)], Xinliang Feng (✉)[2, 3], Shixuan Du (✉)[1, 5] and Hong-Jun Gao (✉)[1, 5]

[1] *Beijing National Center for Condensed Matter Physics and Institute of Physics & University of Chinese Academy of Sciences, Chinese Academy of Sciences, Beijing 100190, PR China*

[2] *Center for Advancing Electronics Dresden (cfaed) & Faculty of Chemistry and Food Chemistry, Technische Universität Dresden, D-01069 Dresden, Germany*

[3] *Max Planck Institute of Microstructure Physics, Weinberg 2, Halle, 06120 Germany*

[4] *Department of Chemistry, State Key Laboratory of Synthetic Chemistry, The University of Hong Kong, Pokfulam Road, Hong Kong, China*

[5] *Songshan Lake Materials Laboratory, Dongguan, Guangdong 523808, PR China*

[§] *Xiao Chang, Li Huang, Yixuan Gao and Yubin Fu contributed equally to this work.*

Received: day month year / **Revised:** day month year / **Accepted:** day month year (automatically inserted by the publisher)

Contents

■ (i) Synthesis and Characterization of BDBT

1. Experimental details

General methods and materials: All the reagents were obtained from Sigma Aldrich, TCI, abcr, Alfa Aesar and Strem. All these chemicals were used as received without further purification. Anhydrous tetrahydrofuran (THF) and dichloromethane (DCM) were obtained from MBRAUN MB-SPS-5 solvent purification system and anhydrous *o*-dichlorobenzene (*o*-DCB) was obtained from Acros organics. All the sensitive reactions were performed using standard vacuum-line and Schlenk techniques. Thin layer chromatography (TLC) was performed on silica-coated aluminum sheets with a fluorescence indicator (TLC silica gel 60 F_{254}, purchased from Merck KGaA). Column chromatography was performed on silica (SiO_2, particle size 0.063−0.200 mm, purchased from VWR). NMR spectra were recorded on a Bruker AV-II 300 spectrometer operating at 300 MHz for ^{1}H, 76 MHz for ^{13}C and 96 MHz for ^{11}B with standard Bruker pulse programs at room temperature (296 K). ^{11}B NMR chemical shifts were referenced to the external standard boron signal of boron trifluoride etherate ($BF_3{\cdot}Et_2O$) ($\delta = 0$ ppm). Dichloromethane-d_2 (CD_2Cl_2) (^{1}H, $\delta = 5.32$ ppm, ^{13}C, $\delta = 53.8$ ppm) was used as solvent and TMS ($\delta_{TMS} = 0.0$ ppm) was used as internal standard. The following abbreviations are used to describe peak patterns as appropriate: s = singlet, d = doublet, t = triplet, q = quartet, and m = multiplet. CD_2Cl_2 (99.9 atom% D) was purchased from Aldrich. The mass spectrometry analysis was performed on a Bruker Autoflex Speed MALDI TOF MS (Bruker Daltonics, Bremen, Germany) using DCTB (trans-2-[3-(4-*tert*-butylphenyl)-2-methyl-2-propenylidene]malononitrile) as matrix or Agilent Q-TOF (APCI mode using acetonitrile as solvent) instruments.

2. Synthetic procedures

(4'-isopropyl-[1,1'-biphenyl]-4-yl)trimethylsilane (2).

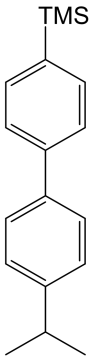

In a 250 mL three-necked round flask, (4-bromophenyl)trimethylsilane (5.00 g, 21.81 mmol), (4-isopropylphenyl)boronic acid **1** (5.37 g, 32.70 mmol), and K_2CO_3 (12.00 g, 87.20 mmol) were charged under the protection of argon. After adding 70 mL toluene, ethanol, and H_2O (5:1:1) the mixture was degassed under argon for 30 min. Then $Pd(PPh_3)_4$ (1.25 g, 1.09 mmol) was charged under the protection of argon and the mixture was heated to 80 °C and stirred for 24 hours. After cooling down to room temperature, the reactant was poured into brine and extracted by dichloromethane for three times. The organic phase was dried over magnesium sulfate and the solvent was evaporated in vacuo. The crude product was purified by flash chromatography on silica gel (CH_2Cl_2/iso-hexane = 1/5) to give product as colorless oil (5.63 g, 96 %). ^{1}H NMR (300 MHz, CD_2Cl_2) δ 7.65 – 7.51 (m, 6H), 7.36 – 7.28 (m, 2H), 3.04 – 2.90 (m, 1H), 1.32 (s, 3H), 1.30 (s, 3H), 0.36 – 0.30 (m, 9H); ^{13}C NMR (76 MHz, CD_2Cl_2) δ 148.7, 148.2, 141.8, 139.3, 138.9, 138.9, 134.2, 127.3, 127.3, 127.2, 127.1, 126.6, 34.2, 24.2, -1.0. HRMS (ACPI, m/z): calcd for $C_{18}H_{24}Si^+$ $[M]^+$ 268.1647, found 268.1648.

(4'-isopropyl-[1,1'-biphenyl]-4-yl)boronic acid (3).

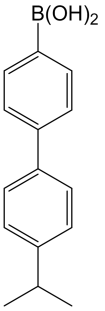

In a 100 mL three-necked round flask, compound **2** (5.63 g, 20.97 mmol) and neat boron tribromide (3.4 mL, 35.83 mmol) were charged under the protection of argon. Then the mixture was heated to 100 °C and stirred for 4 hours. After cooling down to room temperature, excess boron tribromide was distilled off under vacuum. The resulting gray-purple solid was dissolved in dry hexane (50 mL) and cooled to 0 °C with an ice bath. Deionized water (20 mL) was slowly added drop wise into the flask while stirring vigorously until the reaction had been fully quenched. The resulting mixture was filtered and the solid product was washed with deionized water and hexane. The powder was then dried at 80 °C under vacuum overnight, yielded product as white powder (4.41 g, 88 %). ^{1}H NMR (300 MHz, DMSO-d_6) δ 8.05 (s,

1H), 7.86 (d, J = 8.2 Hz, 2H), 7.62 (d, J = 1.1 Hz, 2H), 7.59 (d, J = 1.2 Hz, 2H), 7.33 (d, J = 8.2 Hz, 2H), 3.06 – 2.80 (m, 1H), 1.24 (s, 3H), 1.22 (s, 3H); ^{11}B NMR (96 MHz, DMSO-d_6) δ 18.89; ^{13}C NMR (76 MHz, DMSO-d_6) δ 147.8, 141.6, 137.7, 134.7, 126.8, 126.6, 125.4, 33.1, 23.8. Notes: The NMR signal of the carbon adjacent to boron was not observed. HRMS (ACPI, m/z): calcd for $C_{15}H_{17}BO_2^+$ $[M]^+$ 240.1322, found 240.1324.

2',5'-bis(2-nitrophenyl)-[1,1':4',1''-terphenyl]-2,2''-diamine (4).

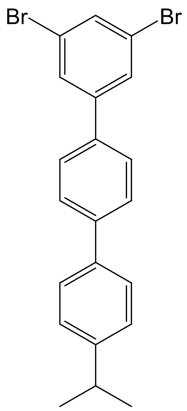

In a 200 mL one-necked flask, compound **3** (1.0101 g, 4.21 mmol), 1,3-dibromo-5-iodobenzene (3.0307 g, 8.37 mmol) and Cs_2CO_3 (6.9622 g, 21.36 mmol) were charged under the protection of argon. After adding 50 mL toluene, ethanol, and H_2O (3:1:1) the mixture was degassed under argon for 30 min. Then $Pd(PPh_3)_4$ (485.7 mg, 0.42 mmol) was charged under the protection of argon and the mixture was heated to 80 °C and stirred for 24 hours. After cooling down to room temperature, the reactant was poured into brine and extracted by dichloromethane for three times. The organic phase was dried over magnesium sulfate and the solvent was evaporated in vacuo. The crude product was purified by flash chromatography on silica gel (CH_2Cl_2/iso-hexane = 1/4) to give product as light red powder (1.65 g, 91 %). ^{1}H NMR (300 MHz, CD_2Cl_2) δ 7.75 (d, J = 1.7 Hz, 2H), 7.72 – 7.70 (m, 1H), 7.69 – 7.66 (m, 2H), 7.63 – 7.61 (m, 1H), 7.61 – 7.59 (m, 2H), 7.58 – 7.56 (m, 1H), 7.37 – 7.35 (m, 1H), 7.34 – 7.32 (m, 1H), 2.98 (hept, J = 6.9 Hz, 1H), 1.32 (s, 3H), 1.30 (s, 3H); ^{13}C NMR (76 MHz, CD_2Cl_2) δ 149.0, 144.7, 141.5, 137.9, 137.0, 132.9, 129.1, 127.8, 127.7, 127.4, 127.2, 123.6, 34.2, 24.1. HRMS (ACPI, m/z): calcd for $C_{21}H_{18}Br_2^+$ $[M]^+$ 427.9775, found 427.9777.

2,2'-(4''-isopropyl-[1,1':4',1''-terphenyl]-3,5-diyl)bis(4,4,5,5-tetramethyl-1,3,2-dioxabor-olane) (5):

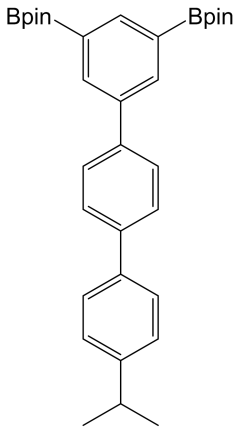

In a 200 mL long-necked Schlenk flask, compound **4** (1.6498 g, 3.84 mmol), 4,4,4',4',5,5,5',5'-octamethyl-2,2'-bi(1,3,2-dioxaborolane) (2.80 g, 11.03 mmol), KOAc (2.09 g, 21.29 mmol), and Pd(dppf)Cl_2 (205.2 mg, 0.25 mmol) were charged under the protection of argon. After adding 30 mL degassed DMSO the mixture was heated to 100 °C and stirred for 24 hours. After cooling down to room temperature, the reactant was poured into brine and extracted by ethyl acetate for three times. The organic phase was dried over magnesium sulfate and the solvent was evaporated in vacuo. The crude product was purified by flash chromatography on silica gel (ethyl acetate/iso-hexane = 1/2) then recrystallized from n-hexane to give product as white powder (1.4702 g, 73 %). ^{1}H NMR (300 MHz, CD_2Cl_2) δ 8.16 (s, 3H), 7.78 – 7.72 (m, 2H), 7.72 – 7.66 (m, 2H), 7.64 – 7.57 (m, 2H), 7.37 – 7.31 (m, 2H), 2.98 (hept, J = 6.9 Hz, 1H), 1.37 (s, 24H), 1.32 (s, 3H), 1.29 (s, 3H); ^{11}B NMR (96 MHz, CD_2Cl_2) δ 30.21; ^{13}C NMR (76 MHz, CD_2Cl_2) δ 148.7, 140.6, 140.3, 139.9, 139.6, 138.4, 136.2, 127.8, 127.5, 127.3, 127.2, 84.3, 34.2, 25.1, 24.1. Notes: The NMR signal of the carbon adjacent to boron was not observed. HRMS (MADLI-TOF, m/z): calcd for $C_{33}H_{42}B_2O_4^+$ $[M]^+$ 524.3269, found 524.3271.

2-bromo-5'-(2-bromo-6-nitrophenyl)-4'''-isopropyl-6-nitro-1,1':3',1'':4'',1'''-quaterphen-yl (6):

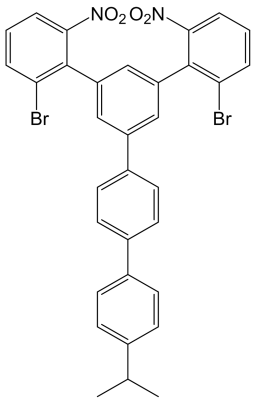

In a 200 mL long-necked Schlenk flask, compound **5** (800.9 mg, 1.53 mmol), 1-bromo-2-iodo-3-nitrobenzene (1.3457 mg, 4.10 mmol), Na_2CO_3 (1.8388 g, 17.35 mmol), and $Pd(dppf)Cl_2$ (98.1 mg, 0.12 mmol) were charged under the protection of argon. After adding 32 mL degassed THF and H_2O (3:1) the mixture was heated to 70 °C and stirred for 12 hours. After cooling down to room temperature, the reactant was poured into brine and extracted by dichloromethane for three times. The organic phase was dried over magnesium sulfate and the solvent was evaporated in vacuo. The crude product was purified by flash chromatography on silica gel (CH_2Cl_2/iso-hexane = 1/2) to give product as light-yellow oily liquid, which solidified slowly (598.3 mg, 58 %). ^{1}H NMR (300 MHz, CD_2Cl_2) δ 7.99 (dd, J = 2.2, 1.2 Hz, 1H), 7.96 (dd, J = 2.2, 1.2 Hz, 1H), 7.87 (ddd, J = 8.1, 4.4, 1.1 Hz, 2H), 7.75 – 7.66 (m, 4H), 7.60 (d, J = 1.6 Hz, 2H), 7.59 – 7.56 (m, 2H), 7.45 (td, J = 8.1, 1.1 Hz, 2H), 7.34 (s, 1H), 7.32 (s, 1H), 7.15 (dt, J = 8.3, 1.5 Hz, 1H), 3.04 – 2.88 (m, 1H), 1.30 (s, 3H), 1.28 (s, 3H); ^{13}C NMR (76 MHz, CD_2Cl_2) δ 151.2, 148.9, 141.4, 141.0, 138.5, 138.1, 137.5, 137.2, 137.1, 136.1, 136.0, 130.2, 130.1, 128.8, 128.9, 127.8, 127.7, 127.6, 127.6, 127.3, 127.2, 126.4, 126.3, 123.2, 123.1, 34.2, 24.1. Notes: The ^{13}C NMR spectrum of compound **6** exhibits more than 20 peaks. This is also caused by the presence of conformational isomers (the different rotation angle of the side substitution groups). This result is in line with our reported molecules[1] and these isomers will not affect the following reactions. HRMS (MADLI-TOF, m/z): calcd for $C_{33}H_{24}Br_2N_2O_4^+$ $[M]^+$ 670.0103, found 670.0101.

(5''-(4'-isopropyl-[1,1'-biphenyl]-4-yl)-3',6'''-dinitro-[1,1':2',1'':3'',1''':2''',1''''-quinque-phenyl]-4,4''''-diyl)bis(trime thylsilane) (7):

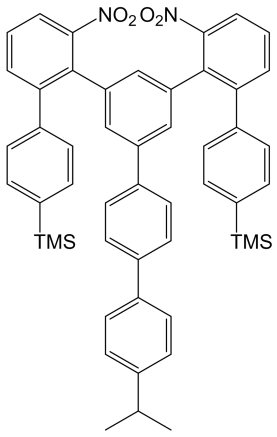

In a 200 mL long-necked Schlenk flask, compound **6** (498.3 mg, 0.74 mmol), (4-(trimethylsilyl)phenyl)boronic acid (757.0 mg, 3.90 mmol), and Cs_2CO_3 (2.5478 g, 7.82 mmol) were charged under the protection of argon. After adding 25 mL toluene, ethanol, and H_2O (3:1:1) the mixture was degassed by Ar for 30 min. Then $Pd(PPh_3)_4$ (123.5 mg, 0.11 mmol) was charged under the protection of argon and the mixture was heated to 80 °C and stirred for 12 hours. After cooling down to room temperature, the reactant was poured into brine and extracted by dichloromethane for three times. The organic phase was dried over magnesium sulfate and the solvent was evaporated in vacuo. The crude product was purified by flash chromatography on silica gel (CH_2Cl_2/iso-hexane = 1/4) to give product as yellow oily liquid, which solidified slowly (500.0 mg, 84 %). ^{1}H NMR (300 MHz, CD_2Cl_2) δ 7.89 – 7.77 (m, 2H), 7.69 (dd, J = 15.6, 5.5 Hz, 2H), 7.60 (dd, J = 14.8, 6.9 Hz, 3H), 7.47 (dd, J = 16.8, 8.1 Hz, 8H), 7.33 (t, J = 9.7 Hz, 2H), 7.11 (d, J = 7.5 Hz, 4H), 6.91 (d, J = 14.9 Hz, 3H), 6.73 (d, J = 7.7 Hz, 1H), 3.05 – 2.87 (m, 1H), 1.30 (s, 3H), 1.28 (s, 3H), 0.27 – 0.23 (m, 18H); ^{13}C NMR (76 MHz, CD_2Cl_2) δ 151.6, 151.1, 148.8, 148.7, 144.4, 143.9, 141.5, 141.2, 140.4, 139.9, 139.8, 139.5, 138.3, 136.7, 136.4, 136.1, 134.2, 133.6, 133.4, 129.7, 129.6, 128.8, 128.6, 127.9, 127.8, 127.6, 127.3, 127.3, 127.1, 126.7, 122.9, 34.2, 24.1, -1.1. Notes: Similar to compound **6**, the ^{13}C NMR spectrum of compound **7** exhibits more than 27 peaks. This is also caused by the presence of conformational isomers (the different rotation angle of the side substitution groups). This result is in line with our reported molecules and these isomers will not affect the following reactions. HRMS (ACPI, m/z): calcd. for $C_{51}H_{50}N_2O_4Si_2^+$ $[M+H]^+$ 810.3309, found 810.3308.

4,4''''-diiodo-5''-(4'-isopropyl-[1,1'-biphenyl]-4-yl)-3',6'''-dinitro-1,1':2',1'':3'',1''':2''', 1''''-quinquephenyl (8):

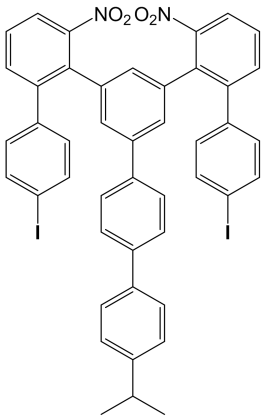

In a 100 mL long-necked Schlenk flask, compound **7** (500.0 mg, 0.62 mmol) was charged under the protection of argon. After adding 15 mL anhydrous DCM the mixture was cooled to 0 °C. ICl (527.4 mg, 3.25 mmol, dissolved in 2 mL anhydrous DCM) was charged under the protection of argon and the mixture was stirred for 10 minutes. Then the ice bath was removed and the resulting mixture was stirred at room temperature for 12 hours. Afterward the reaction was quenched with 50 mL saturated sodium sulfite solution, and extracted by dichloromethane for three times. The organic phase was dried over magnesium sulfate and the solvent was evaporated in vacuo. The crude product was purified by flash chromatography on silica gel (CH_2Cl_2/iso-hexane = 1/2) to give product as light yellow solid (289.8 mg, 50 %). ^{1}H NMR (300 MHz, CD_2Cl_2) δ 7.83 (d, J = 7.5 Hz, 2H), 7.67 (d, J = 7.8 Hz, 5H), 7.62 – 7.54 (m, 5H), 7.53 (s, 1H), 7.45 – 7.35 (m, 1H), 7.35 – 7.18 (m, 2H), 7.15 – 6.95 (m, 5H), 6.87 (d, J = 7.9 Hz, 3H), 6.72 (d, J = 5.9 Hz, 1H), 3.04 – 2.86 (m, 1H), 1.30 (s, 3H), 1.27 (s, 3H). ^{13}C NMR (76 MHz, CD_2Cl_2) δ 151.1, 150.5, 148.8, 143.2, 141.4, 140.7, 139.2, 138.9, 138.8, 138.1, 137.7, 137.5, 136.3, 134.0, 133.4, 132.3, 132.1, 131.5, 130.2, 129.7, 129.1, 128.6, 128.5, 128.3, 127.6, 127.5, 127.3, 127.1, 126.9, 126.5, 125.6, 123.1, 93.8, 34.2, 34.0, 24.1, 23.9. Notes: Similar to compound **6**, the ^{13}C NMR spectrum of compound **8** exhibits more than 26 peaks. This is also caused by the presence of conformational isomers (the different rotation angle of the side substitution groups). This result is in line with our reported molecules[1] and these isomers will not affect the following reactions. HRMS (ACPI, m/z): calcd for $C_{42}H_{26}I_2N_2O_4^+$ $[M]^+$ 918.0451, found 918.0452.

4,4''''-diiodo-5''-(4'-isopropyl-[1,1'-biphenyl]-4-yl)-[1,1':2',1'':3'',1''':2''',1''''-quinqueph-enyl]-3',6'''-diamine (9):

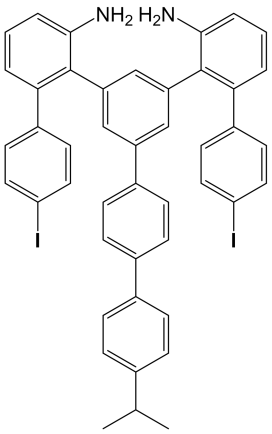

In a 50 mL one-necked flask, compound **8** (269.8 mg, 0.29 mmol) was charged under the protection of argon. Then 16 mL THF and methanol (1:1) was added into the flask. After Pt/C (56.6 mg, 0.29 mmol) was charged under the protection of argon, the mixture was degassed by H_2 for 5 minutes. And the resulting mixture was stirred at room temperature for 12 hours with a H_2 balloon. Afterward the mixture was filtered by celite and the solvent was evaporated in vacuo. The crude yellow oil (249.4 mg, 100 %) can be used directly for next step without purification because it is sensitive to air. HRMS (MADLI-TOF, m/z): calcd for $C_{45}H_{36}I_2N_2^+$ $[M]^+$ 858.0968, found 858.0970.

4,13-bis(4-iodophenyl)-2-(4'-isopropyl-[1,1'-biphenyl]-4-yl)-8*H*,9*H*-8,9-diaza-8a-borabenzo-[*fg*]tetracene (BDBT):

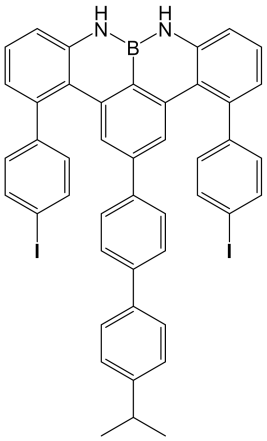

To a solution of compound **9** (236.0 mg, 0.27 mmol) in *o*-dichlorobenzene (15 mL) triethylamine (109.5 mg, 1.08 mmol) and boron tribromide (1 M in n-hexane, 0.41 mL, 0.41 mmol) were added under argon atmosphere. The reaction mixture was heated to 180 °C for 12 h. After cooling to the room temperature, the solvent was evaporated through reduced pressure distillation at 50 °C (0.01 mbar). The residue was then purified by chromatography on silica gel (CH_2Cl_2/iso-hexane = 1/1) then recrystallized two times from $CHCl_3$/MeOH to give product as white powder (52.3 mg, 22%). ^{1}H NMR (300 MHz, $C_2D_2Cl_4$) δ 7.84 (s, 2H), 7.81 (d, *J* = 4.6 Hz, 2H), 7.62 (d, *J* = 7.9 Hz, 2H), 7.58 – 7.39 (m, 4H), 7.38 – 7.33 (m, 2H), 7.30 (d, *J* = 7.7 Hz, 2H), 7.21 (s, 2H), 7.18 (s, 2H), 7.05 (d, *J* = 7.4 Hz, 2H), 6.89 (d, *J* = 7.3 Hz, 2H), 6.63 (d, *J* = 8.3 Hz, 2H), 6.42 (s, 2H), 2.97 (dt, *J* = 14.5, 7.2 Hz, 1H), 1.30 (dd, *J* = 6.9, 2.0 Hz, 6H); ^{13}C NMR (76 MHz, $C_2D_2Cl_4$) δ 148.5, 145.6, 145.6, 142.4, 141.2, 140.0, 139.2, 139.0, 138.7, 138.2, 131.5, 130.6, 128.0, 127.8, 127.5, 127.4,

127.3, 126.6, 125.8, 124.8, 121.1, 118.7, 92.9, 34.2, 34.1, 24.5, 24.3. Notes: The ^{13}C NMR spectrum of **BDBT** shows more than 26 peaks, which may cause by the presence of conformational isomers (the different rotation angle of the side substitution groups). Anyway, for the on-surface reaction there will be no affection. HRMS (MADLI-TOF, m/z): calcd for $C_{45}H_{33}BI_2N_2^+$ $[M]^+$ 866.0826, found 866.0818.

3. NMR spectra

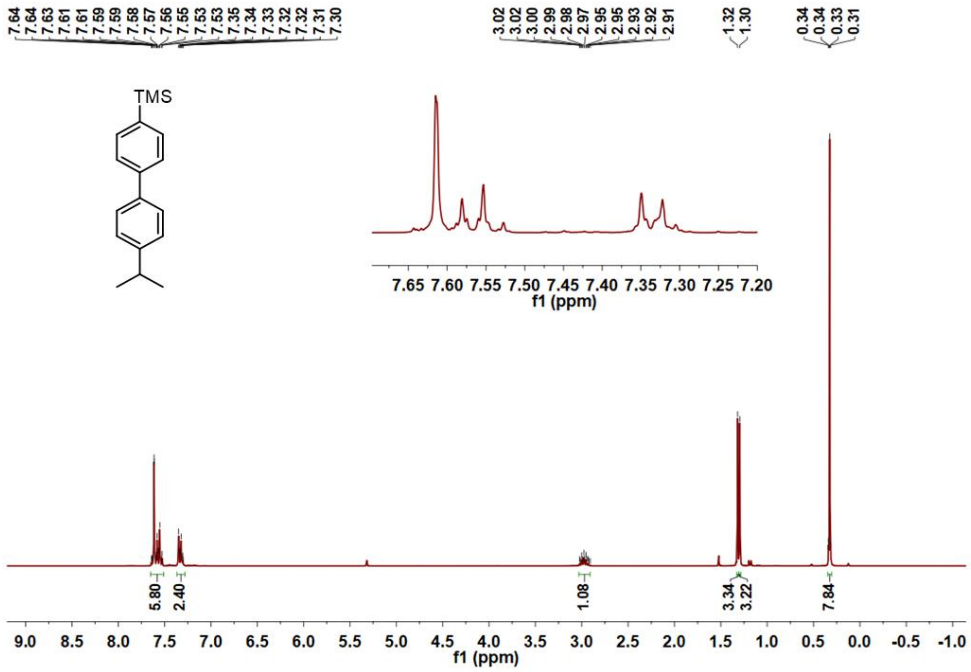

Figure S1: 300 MHz ^{1}H NMR spectrum of compound **2** in CD_2Cl_2 at room temperature.

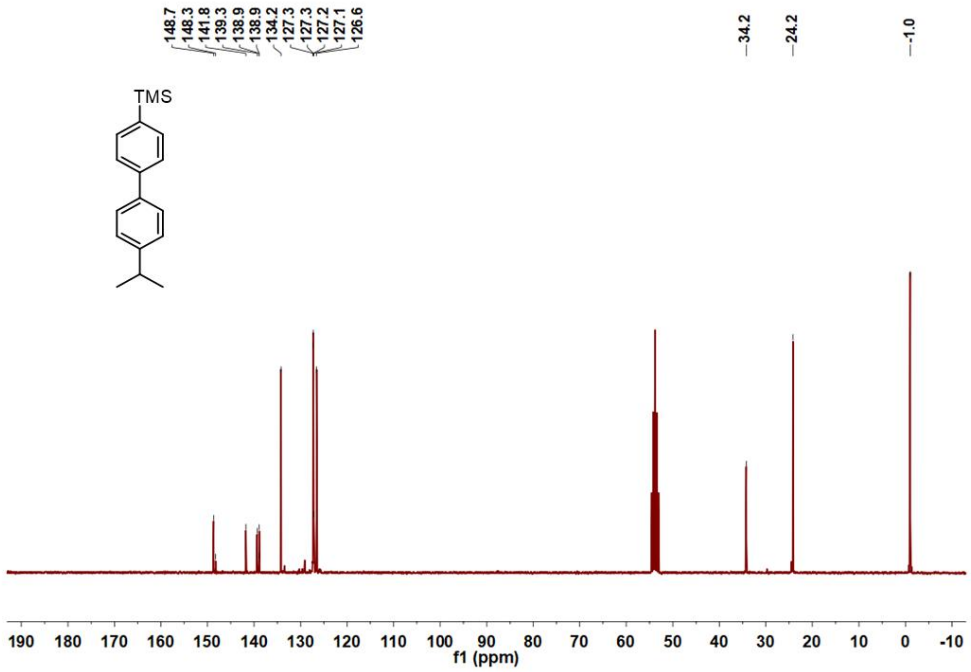

Figure S2: 76 MHz ^{13}C NMR spectrum of compound **2** in CD_2Cl_2 at room temperature.

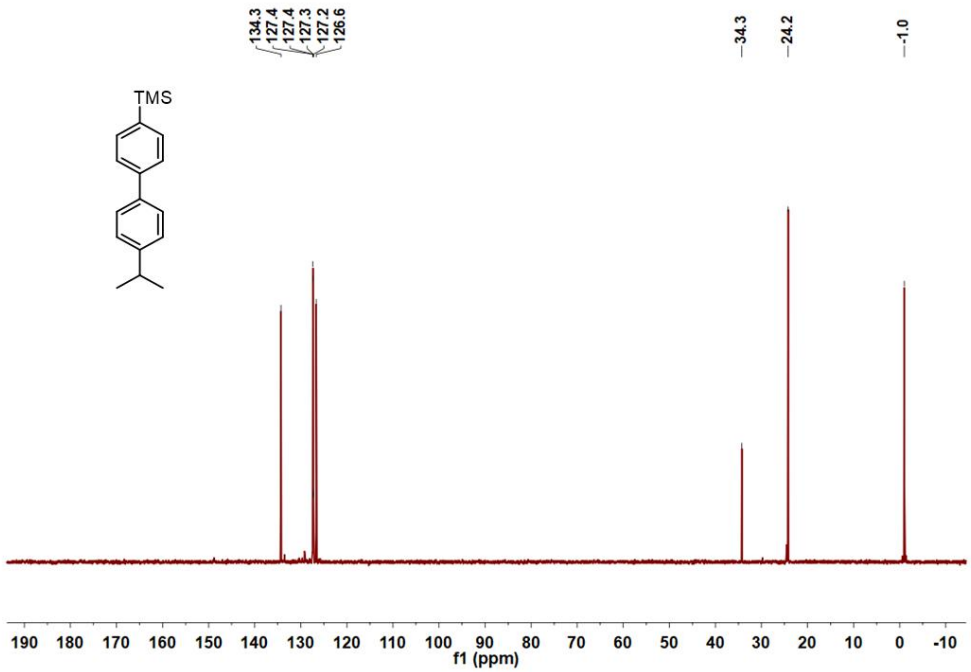

Figure S3: 76 MHz ^{13}C-DEPT-135 NMR spectrum of compound **2** in CD_2Cl_2 at room temperature.

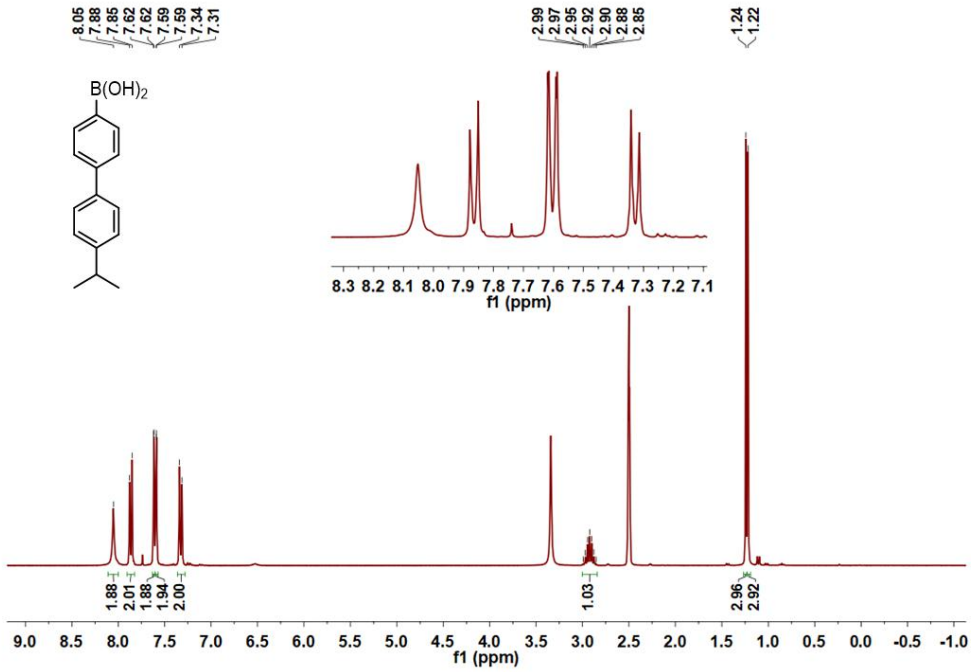

Figure S4: 300 MHz ^{1}H NMR spectrum of compound **3** in CD_2Cl_2 at room temperature.

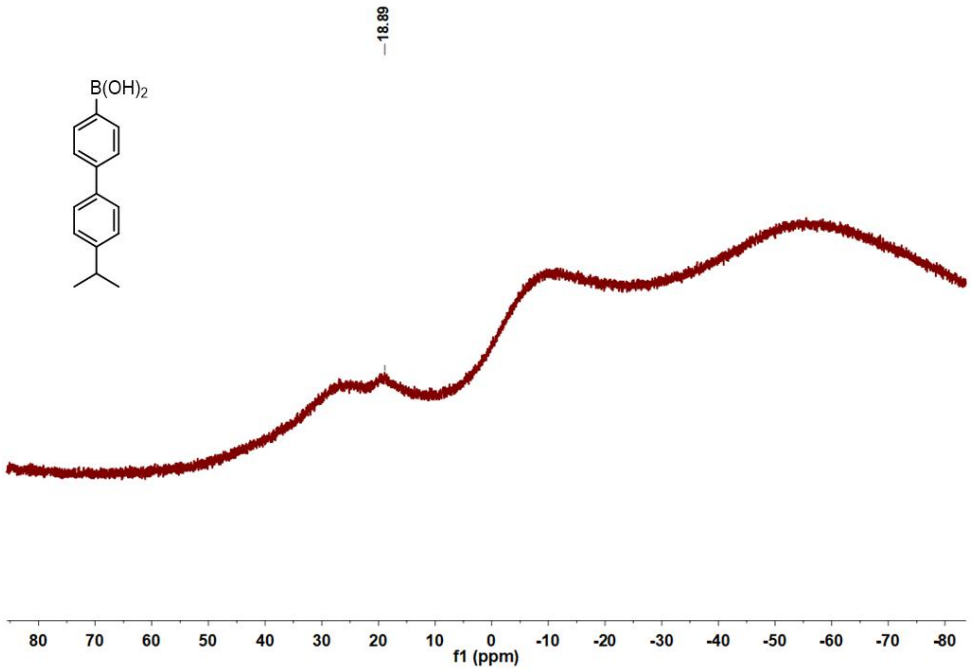

Figure S5: 96 MHz ^{11}B NMR spectrum of compound **3** in CD_2Cl_2 at room temperature.

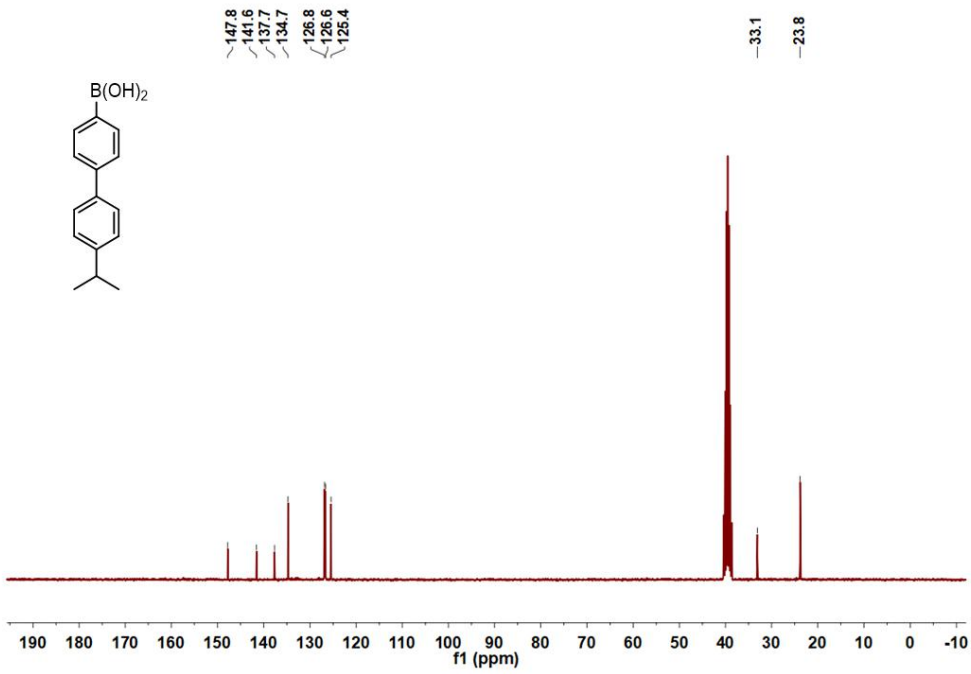

Figure S6: 76 MHz ^{13}C NMR spectrum of compound **3** in CD_2Cl_2 at room temperature.

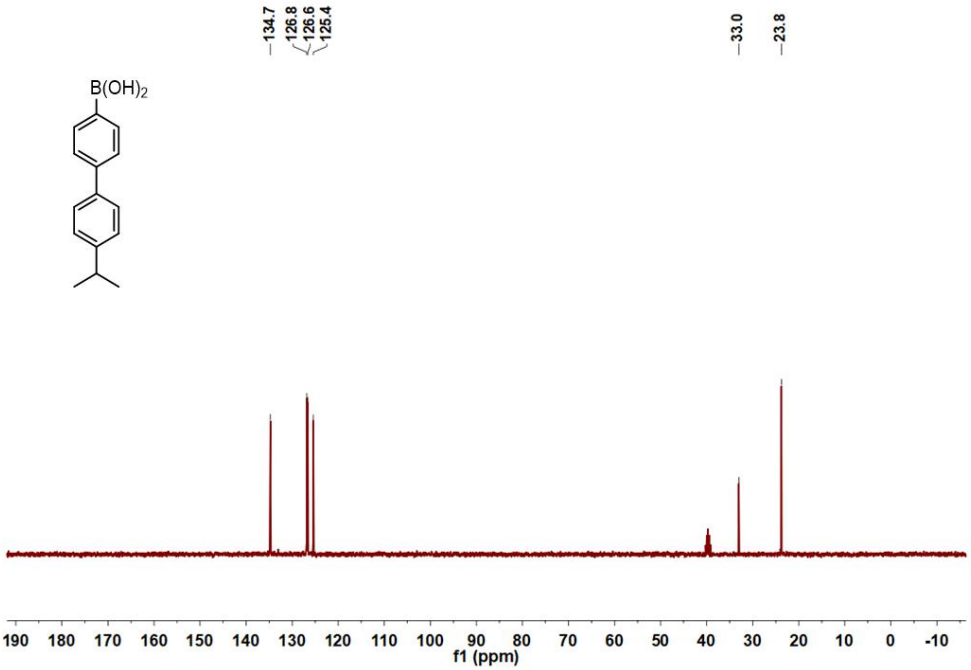

Figure S7: 76 MHz ^{13}C-DEPT-135 NMR spectrum of compound **3** in CD_2Cl_2 at room temperature.

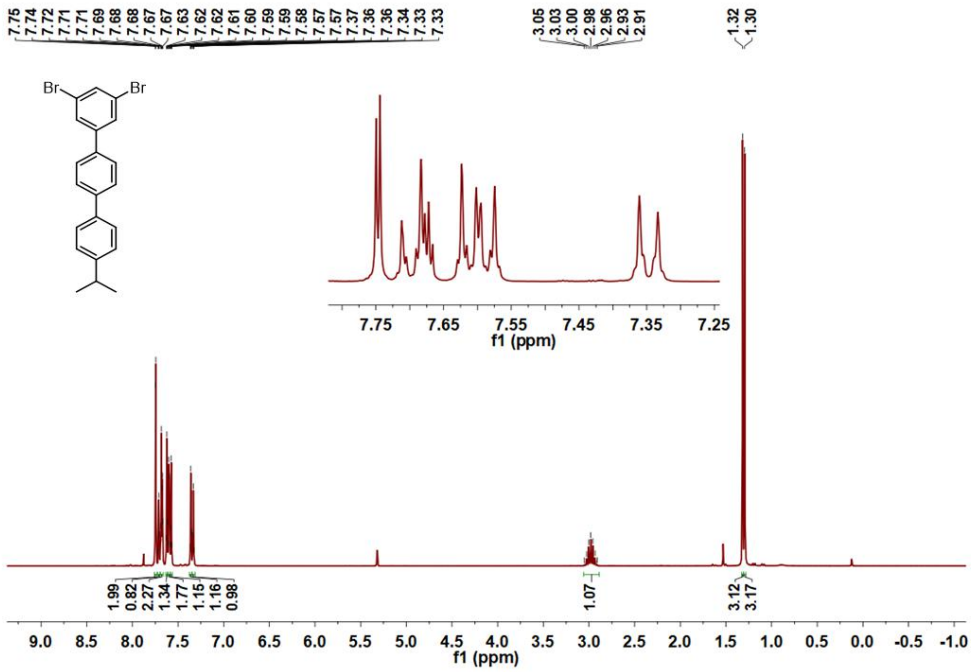

Figure S8: 300 MHz ^{1}H NMR spectrum of compound **4** in CD_2Cl_2 at room temperature.

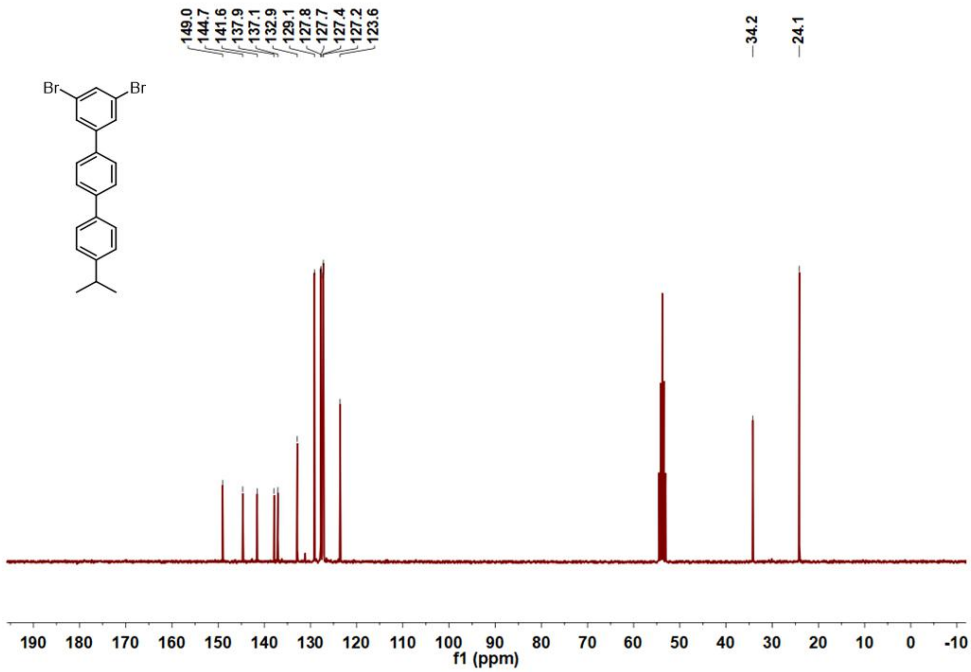

Figure S9: 76 MHz ^{13}C NMR spectrum of compound **4** in CD_2Cl_2 at room temperature.

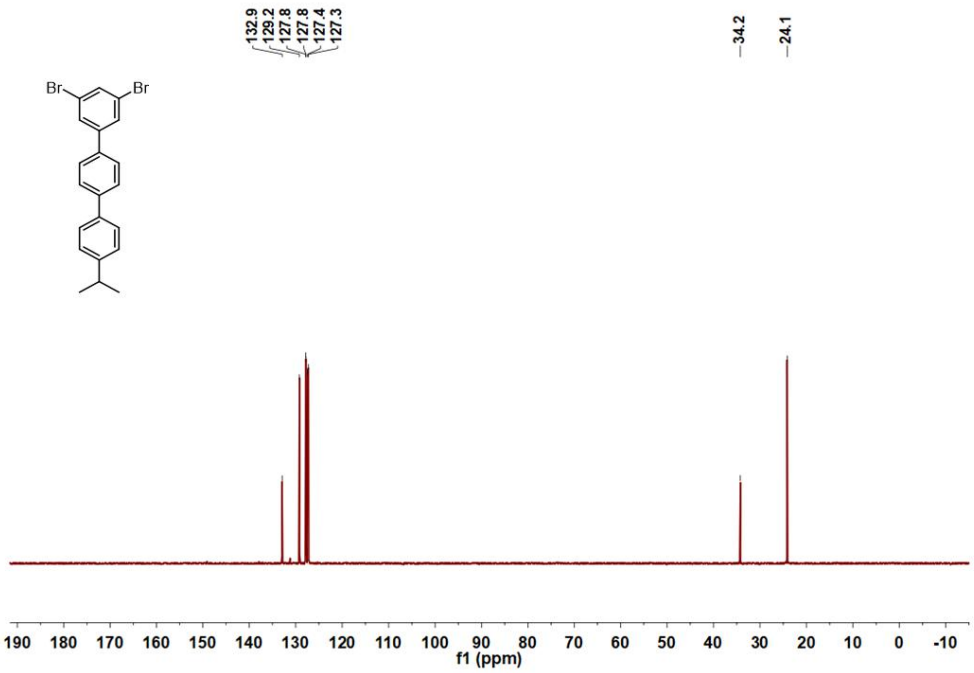

Figure S10: 76 MHz ^{13}C-DEPT-135 NMR spectrum of compound **4** in CD_2Cl_2 at room temperature.

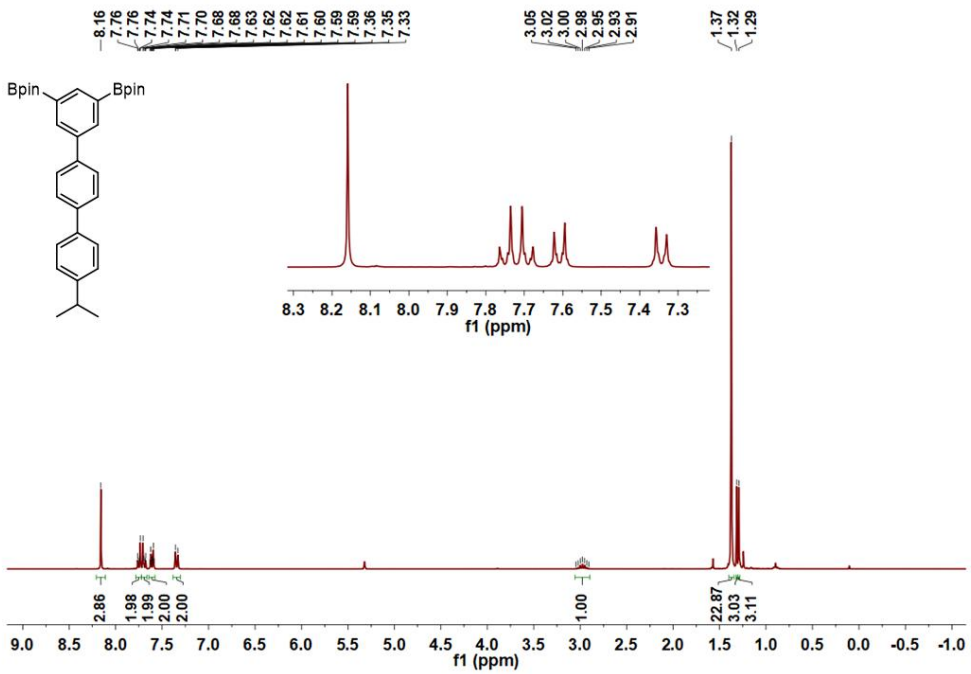

Figure S11: 300 MHz ^{1}H NMR spectrum of compound **5** in CD_2Cl_2 at room temperature.

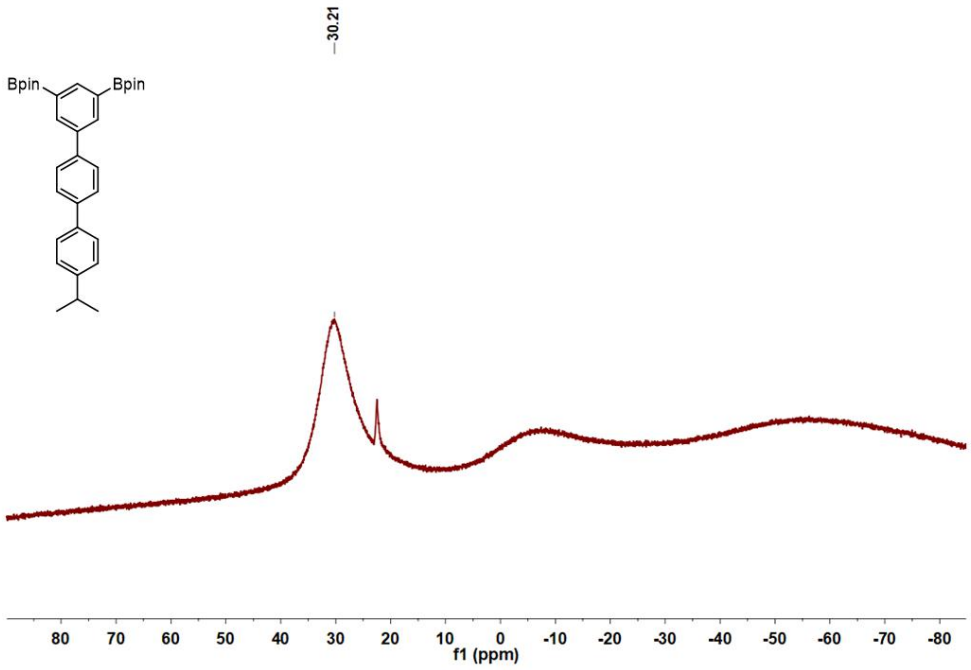

Figure S12: 96 MHz ^{11}B NMR spectrum of compound **5** in CD_2Cl_2 at room temperature.

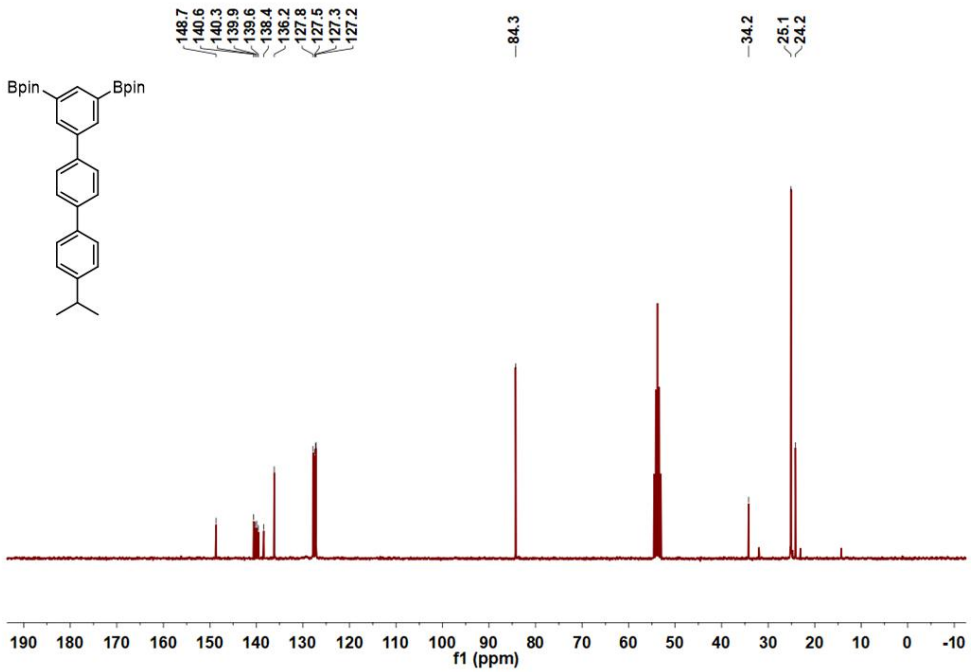

Figure S13: 76 MHz ^{13}C NMR spectrum of compound **5** in CD_2Cl_2 at room temperature.

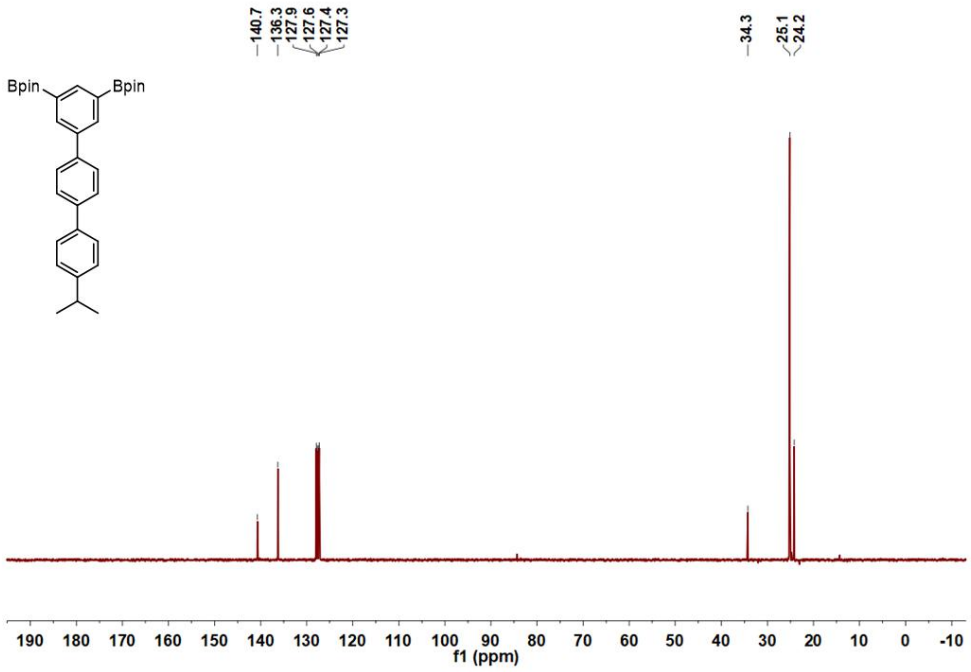

Figure S14: 76 MHz ^{13}C-DEPT-135 NMR spectrum of compound **5** in CD_2Cl_2 at room temperature.

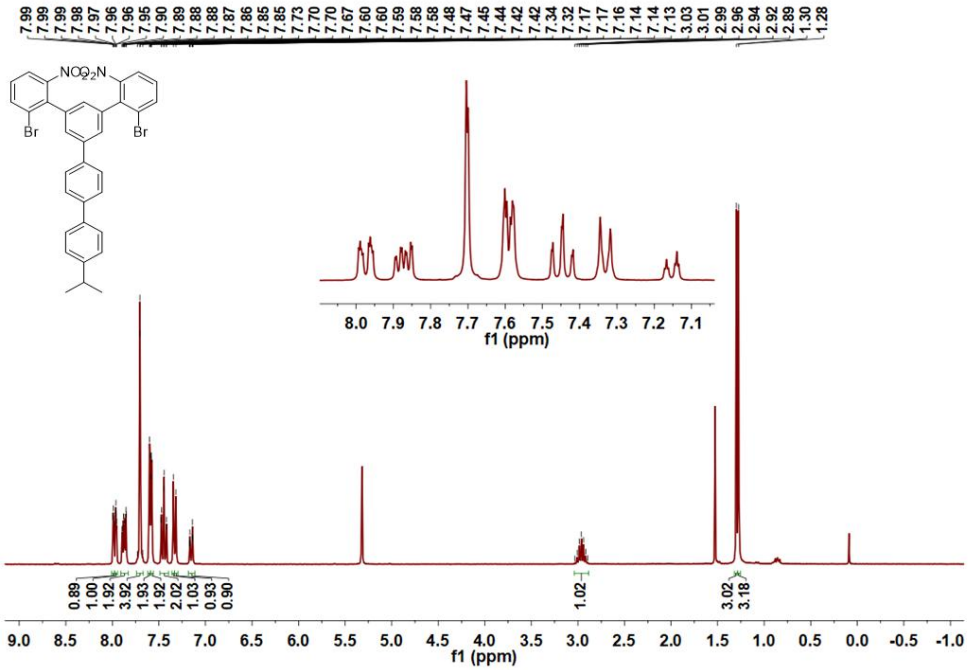

Figure S15: 300 MHz ^{1}H NMR spectrum of compound **6** in CD_2Cl_2 at room temperature.

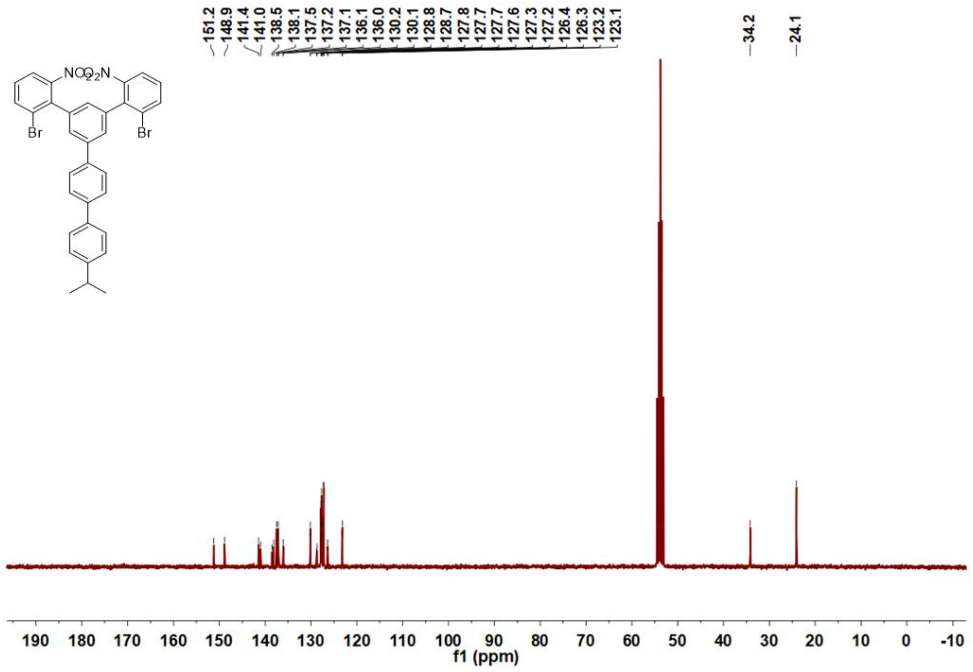

Figure S16: 76 MHz ^{13}C NMR spectrum of compound **6** in CD_2Cl_2 at room temperature.

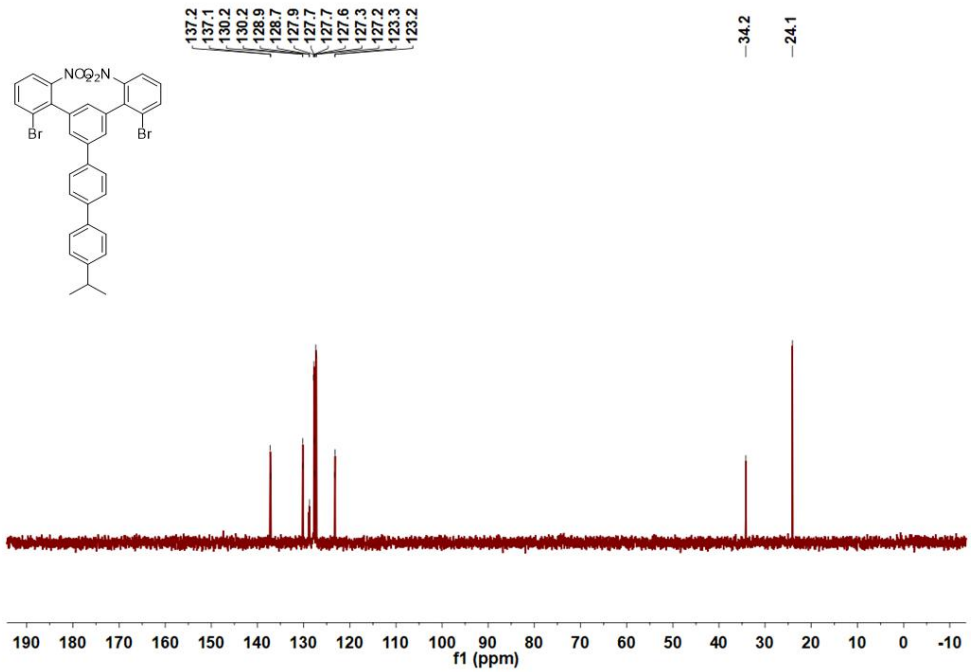

Figure S17: 76 MHz ^{13}C-DEPT-135 NMR spectrum of compound **6** in CD_2Cl_2 at room temperature.

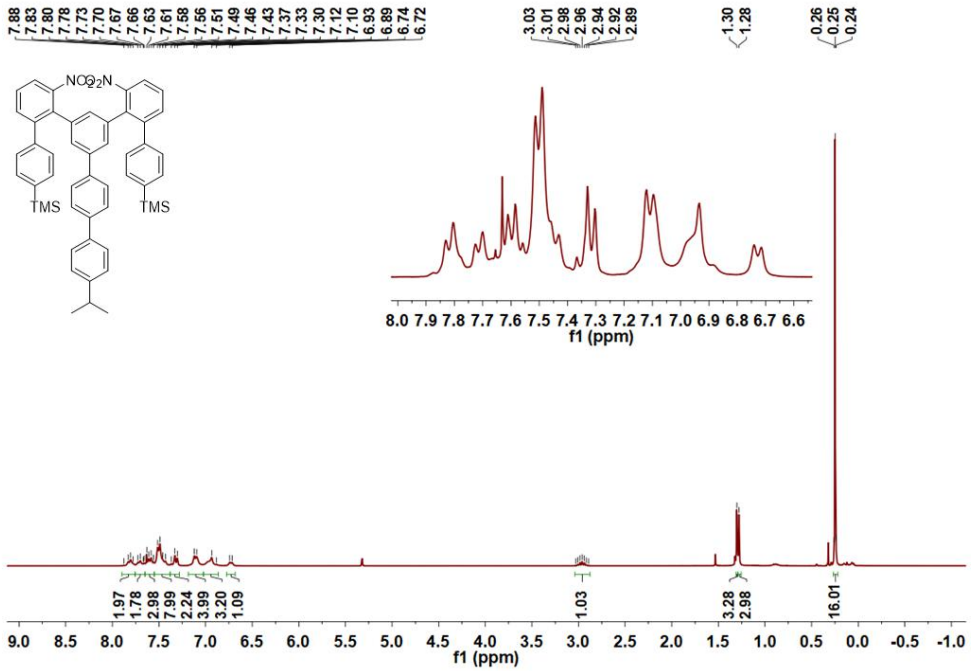

Figure S18: 300 MHz ^{1}H NMR spectrum of compound **7** in CD_2Cl_2 at room temperature.

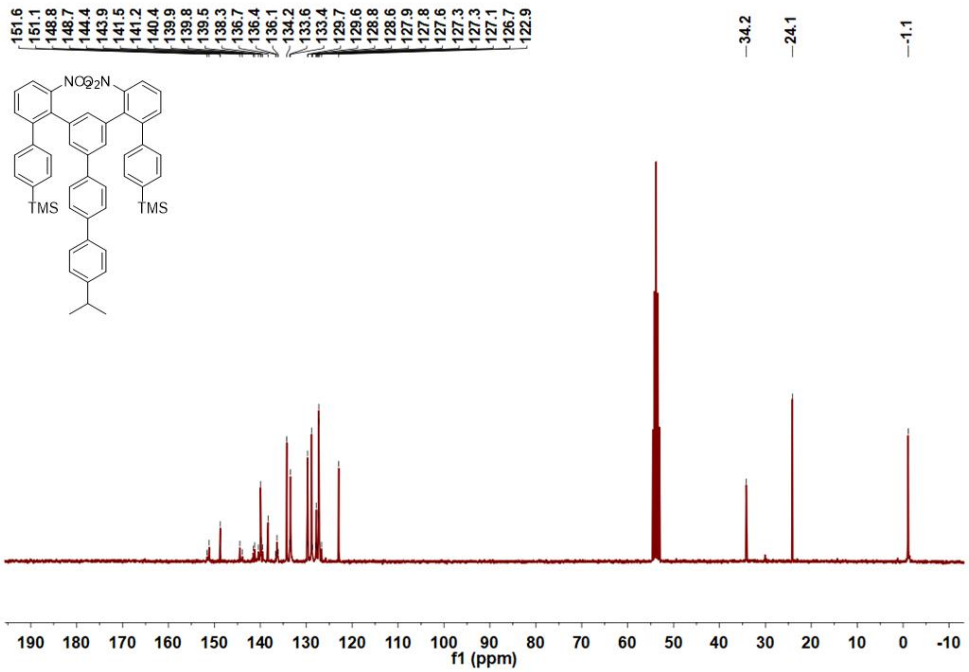

Figure S19: 76 MHz ^{13}C NMR spectrum of compound **7** in CD_2Cl_2 at room temperature.

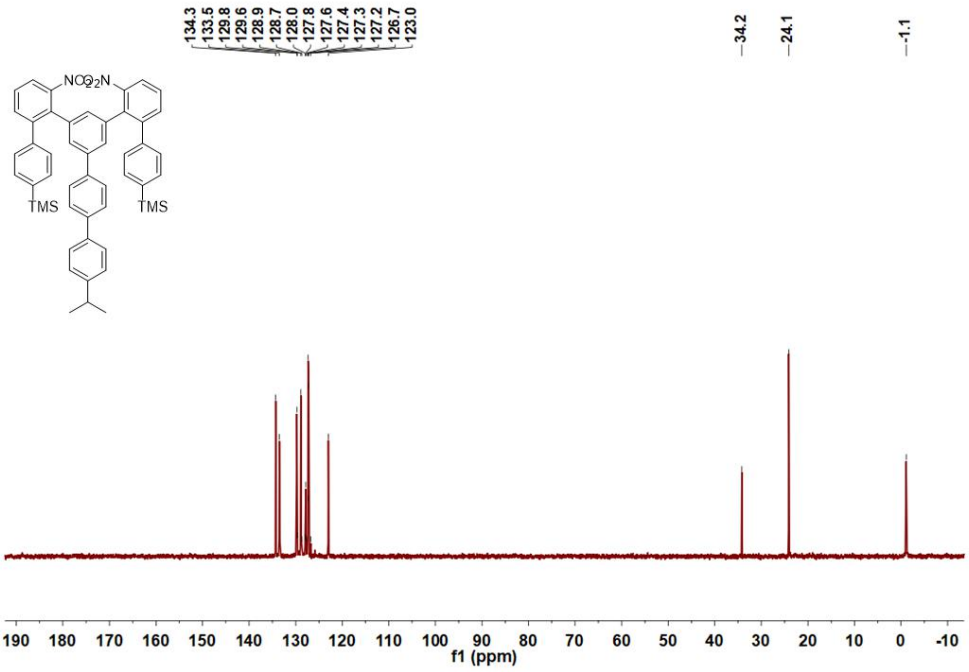

Figure S20: 76 MHz ^{13}C-DEPT-135 NMR spectrum of compound **7** in CD_2Cl_2 at room temperature.

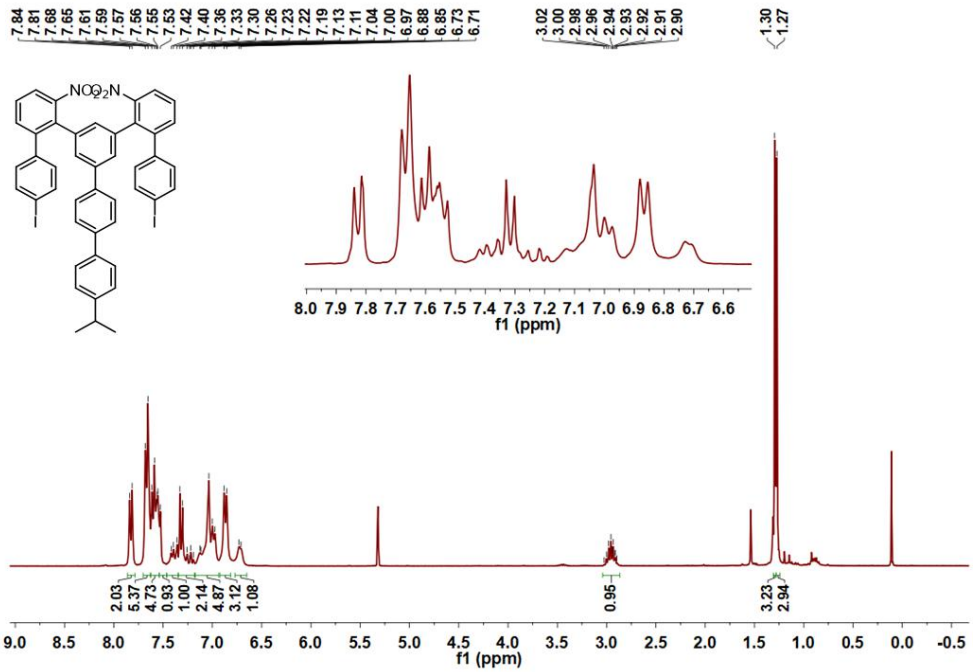

Figure S21: 300 MHz ^{1}H NMR spectrum of compound **8** in CD_2Cl_2 at room temperature.

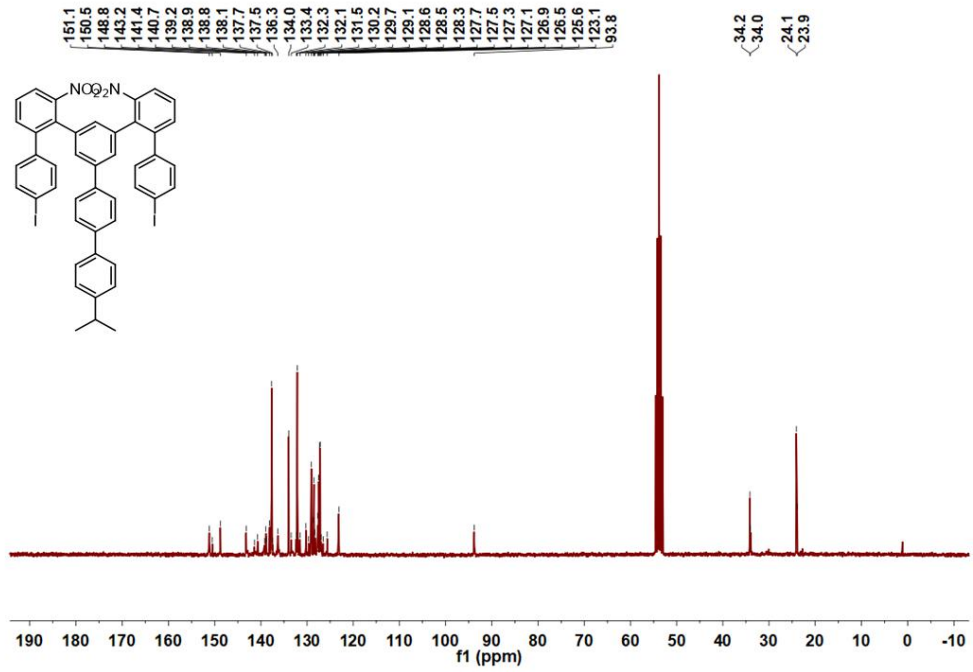

Figure S22: 76 MHz ^{13}C NMR spectrum of compound **8** in CD_2Cl_2 at room temperature.

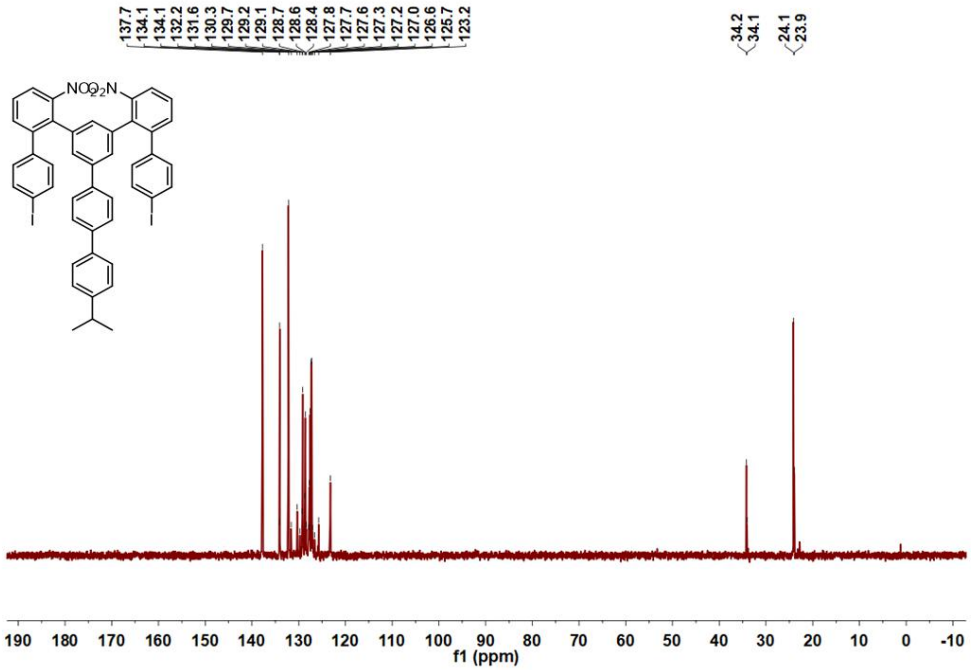

Figure S23: 76 MHz ^{13}C-DEPT-135 NMR spectrum of compound **8** in CD_2Cl_2 at room temperature.

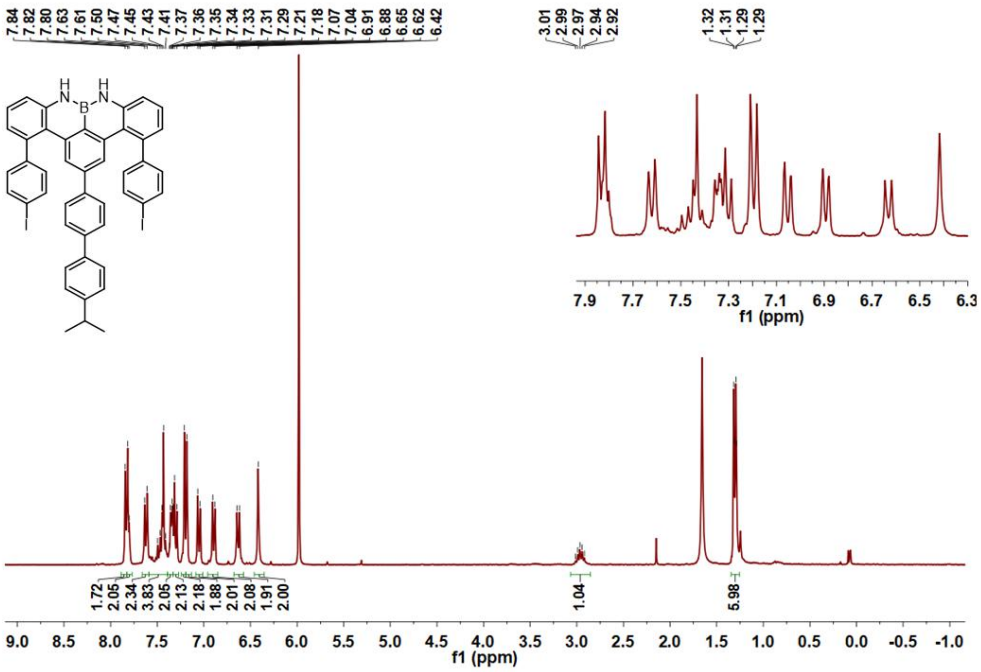

Figure S24: 300 MHz ^{1}H NMR spectrum of **BDBT** in CD_2Cl_2 at room temperature.

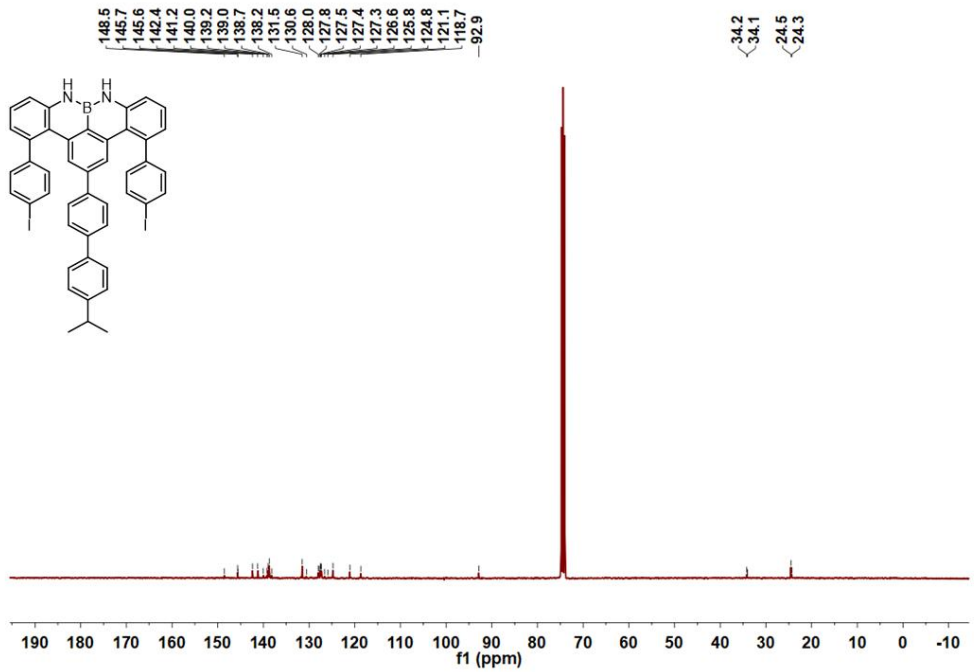

Figure S25: 76 MHz ^{13}C NMR spectrum of **BDBT** in CD_2Cl_2 at room temperature.

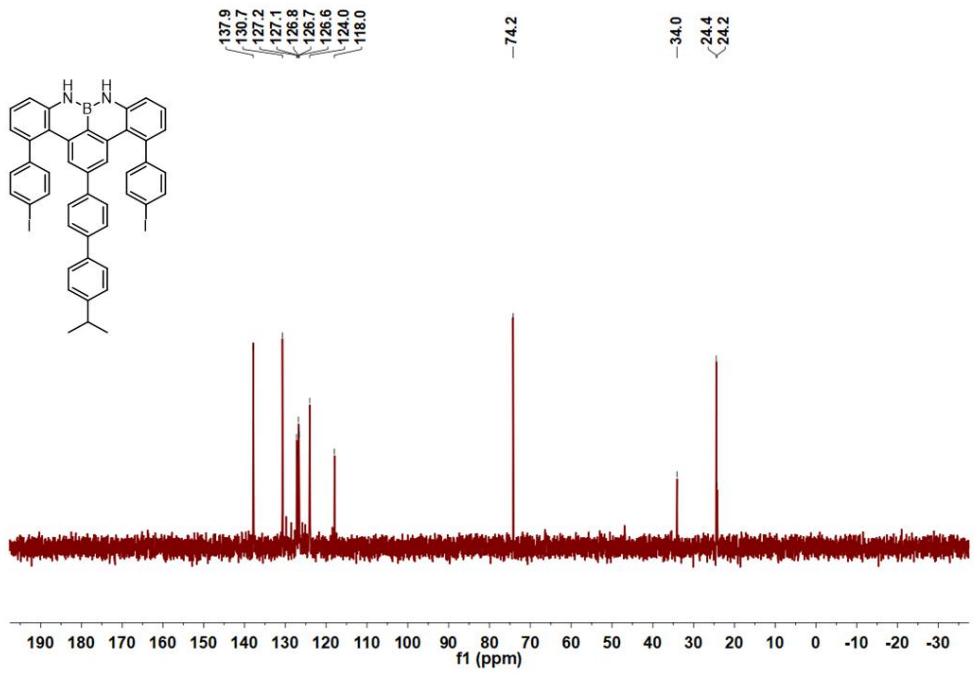

Figure S26: 76 MHz ^{13}C-DEPT-135 NMR spectrum of **BDBT** in CD_2Cl_2 at room temperature.

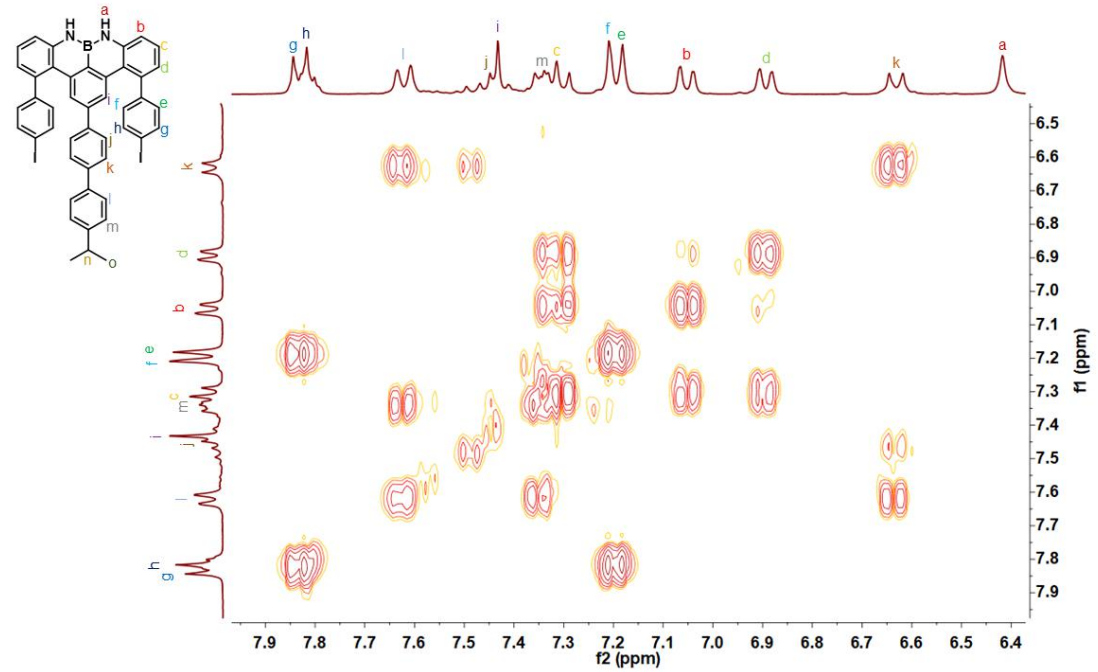

Figure S27: 300 MHz $^{1}H/^{1}H$ COSY spectrum of **BDBT** in CD_2Cl_2 at room temperature.

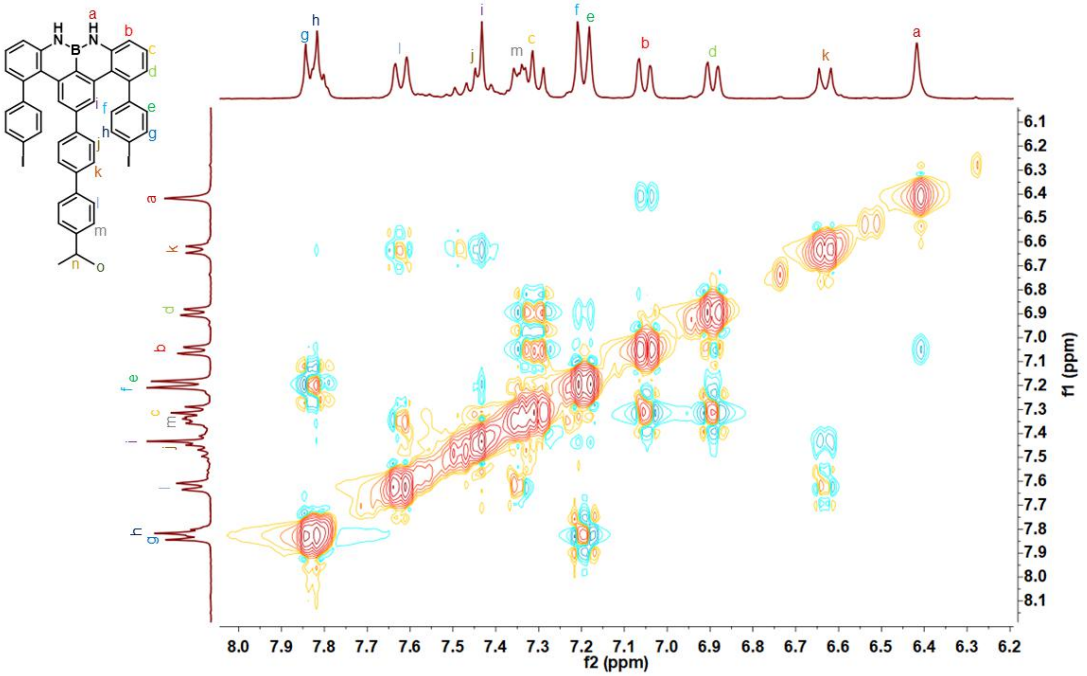

Figure S28: 300 MHz $^{1}H/^{1}H$ NOESY spectrum of **BDBT** in CD_2Cl_2 at room temperature.

4. Mass Spectroscopy (MS)

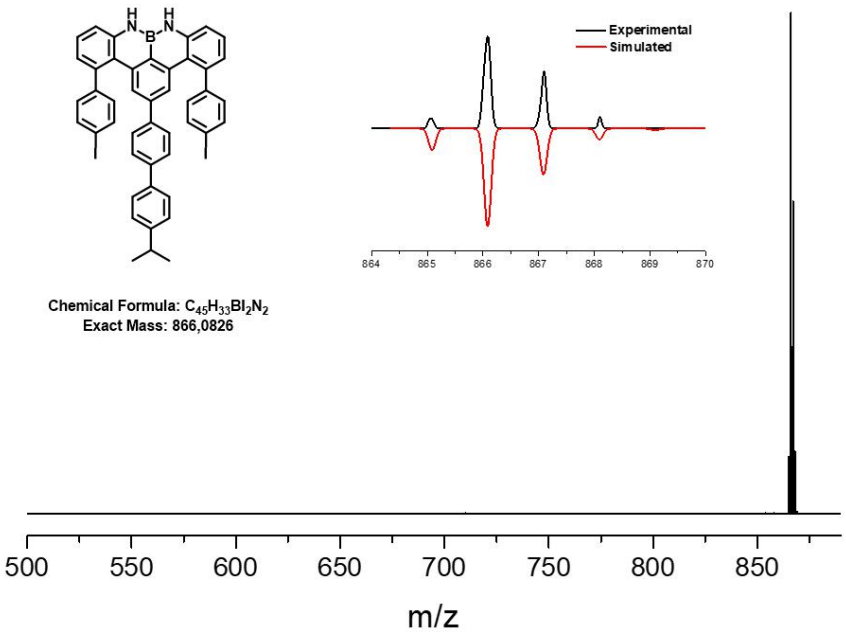

Figure S29: HR-MALDI TOF spectrum of **BDBT** in DCTB.

5. References

[1] Y. Fu, K. Zhang, E. Dmitrieva, F. Liu, J. Ma, J. J. Weigand, A. A. Popov, R. Berger, W. Pisula, J. Liu, X. Feng, *Org. Lett.* **2019**, *21* (5), 1354–1358.

■ (ii) Supplementary Figures

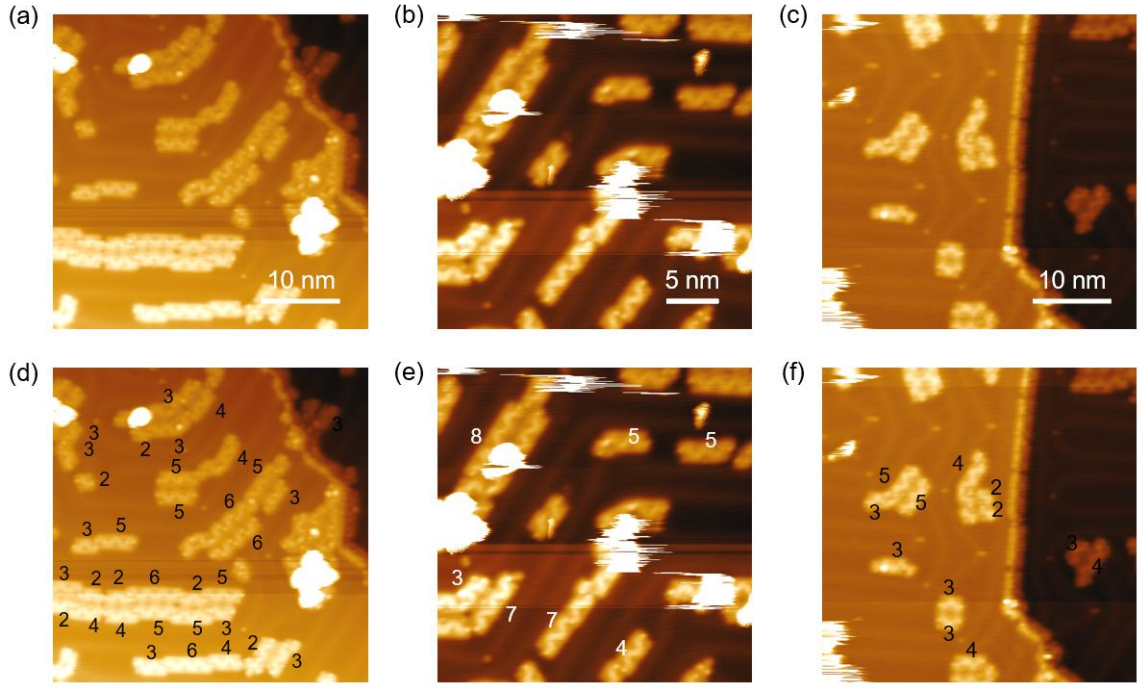

Figure S30 STM images of precursor chains used in the statistical analysis. (a)-(c) Large-scale image of precursor chains on Au(111) surface. (d)-(f) Corresponding images of (a)-(c) with unit number superposed. Scanning parameters: (a) V_s = -1 V, I_t = 30 pA; (b) V_s = -1 V, I_t = 30 pA; (c) V_s = 100 mV, I_t = 50 pA.

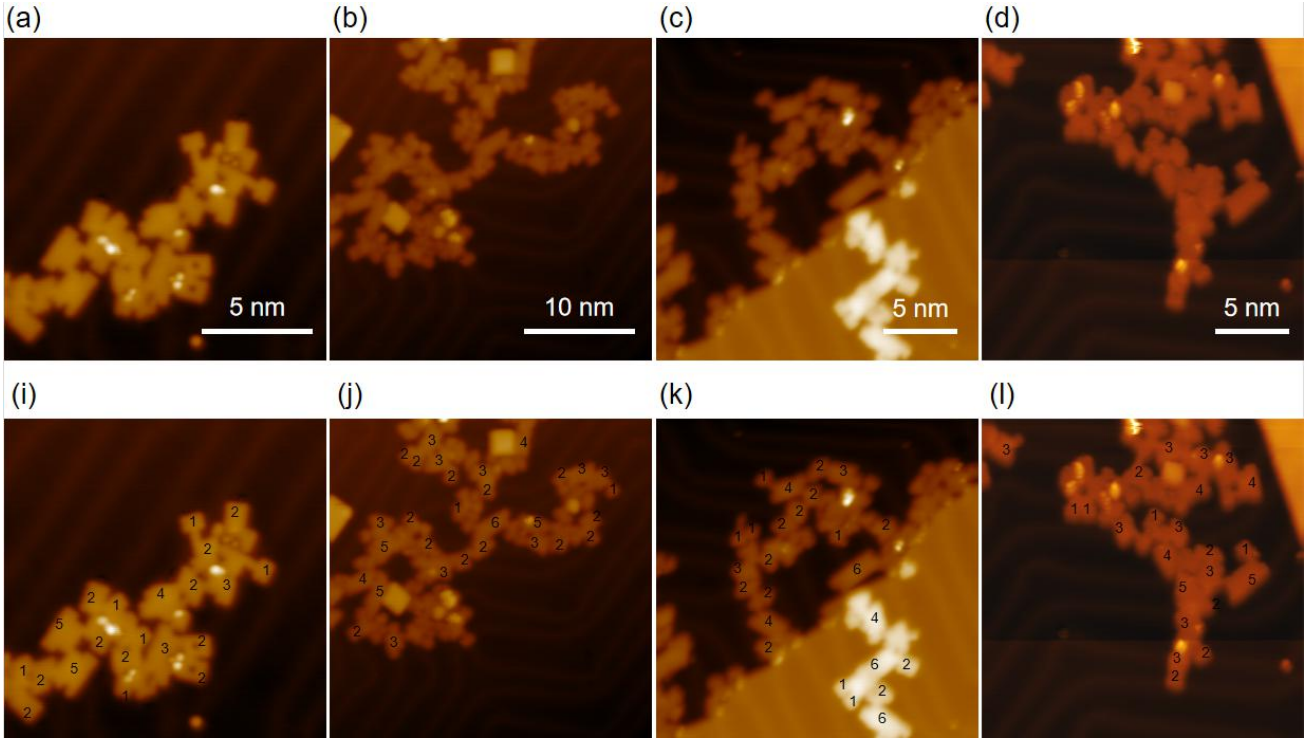

Figure S31 STM images of NBN-8-ZGNRs used in the statistical analysis. (a)-(d) Large-scale images of NBN-8-ZGNRs on Au(111) surface. (i)-(l) Corresponding images of (a)-(d) with number of units superposed. Scanning parameters: (a) V_s = -200 mV, I_t = 10 pA; (b) V_s = -1 V, I_t = 30 pA; (c) V_s = -1 V, I_t = 100 pA; (d) V_s = -1 V, I_t = 200 pA.

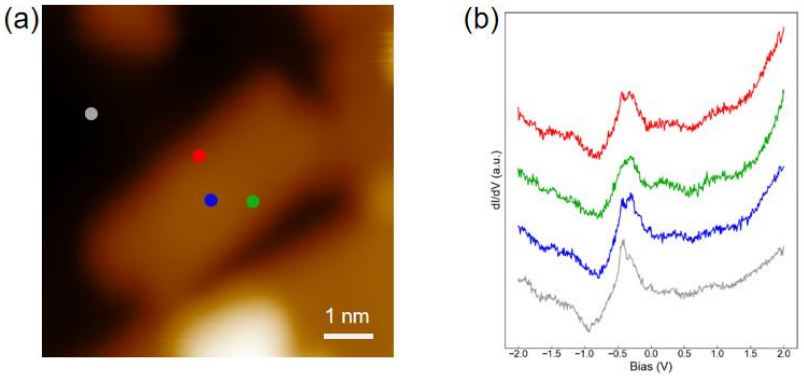

Figure S32 STS of NBN-8-ZGNR on Au(111) substrate. (a) STM image of NBN-8-ZGNR on Au(111) surface (V_s = -1 V, I_t = 100 pA). (b) dI/dV spectra taken on the Au(111) substrate and NBN-8-ZGNR in the same color code as the dots marked in (a). (V_{ac} = 10 mV, modulation frequency = 973 Hz).

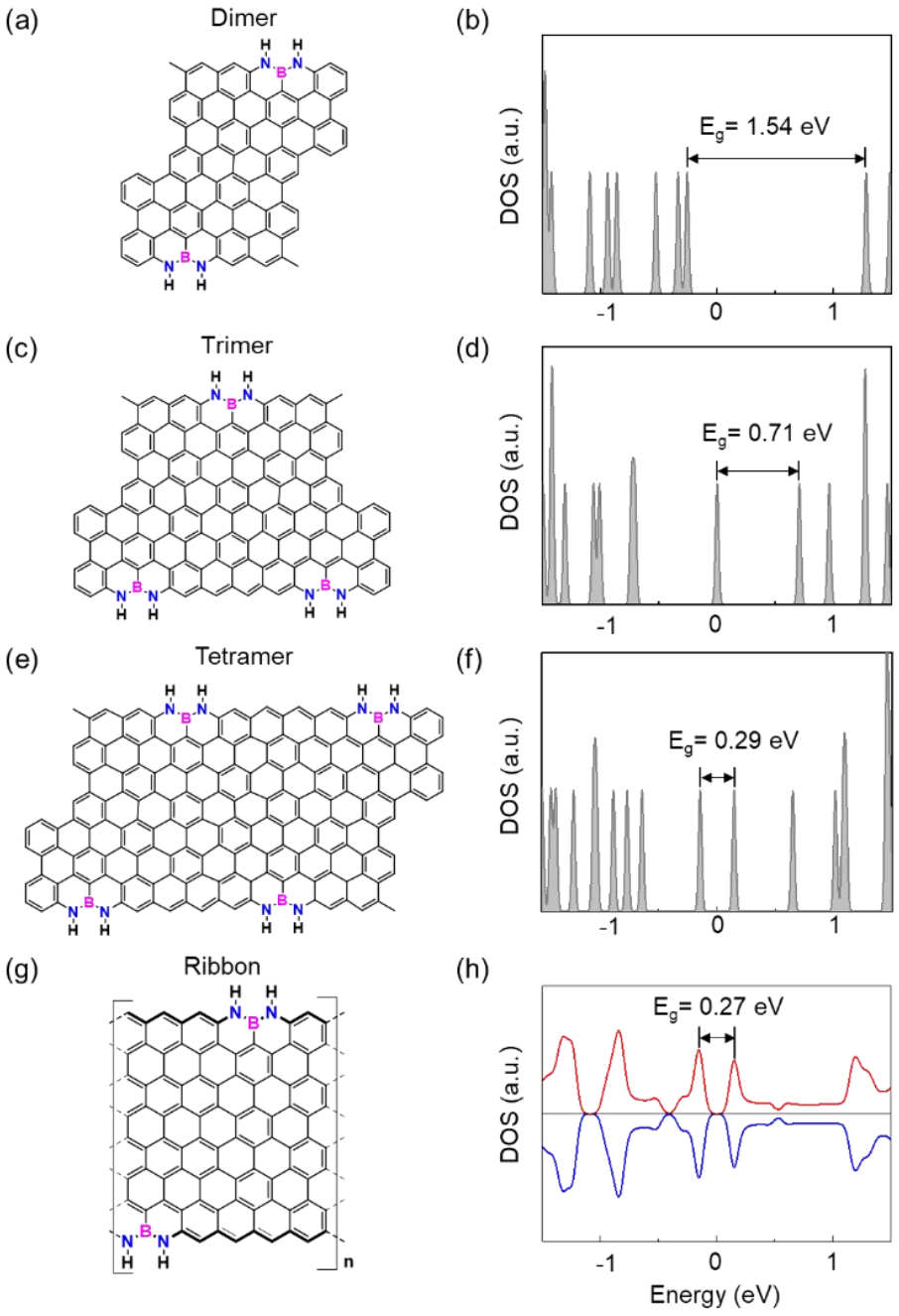

Figure S33 Structural schematic of GNR segments with 2, 3, and 4 units (a, c, e), respectively, and infinite one-dimensional GNR (g). DFT calculated total density of states (DOS) of GNR segments with 2, 3, and 4 units (b, d, f) and infinite one-dimensional GNR (h).

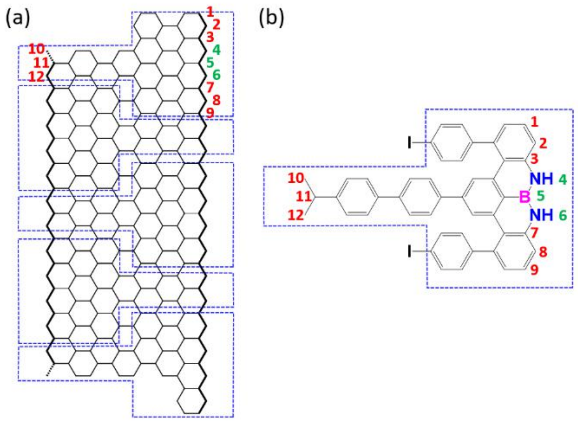

Figure S34 (a) The structure depicted from Fig. 2(f). The T-shaped boxes mark the units that produced by BDBT monomers. The atoms at the zigzag edges produced by one monomer are labeled by numbers 1-12. (b) Chemical structure of a BDBT monomer. The atoms at the zigzag edge and the isopropyl group are labeled with the same order as in (a).

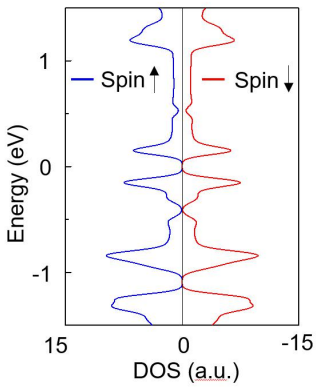

Figure S35 DFT calculated total density of states (DOS) of a freestanding infinite NBN-8-ZGNR ribbon.

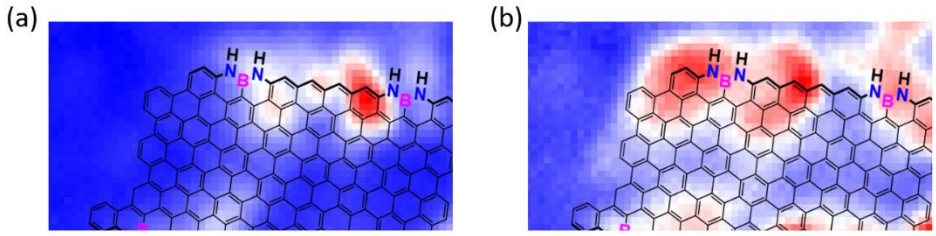

Figure S36 dI/dV maps at the energies of the P1 and P2 states. (a) dI/dV map of the GNR in Fig. 4(c) at the P1 electronic state of -450 mV. (b) dI/dV map of the GNR in Fig. 4(c) at the P2 electronic state of 180 mV. (Parameters for both (a) and (b): frequency = 931 Hz, V_{mod} = 5 mV, before opening feedback loop, V_s = -450 mV, I_t = 1 nA).